Surface mineralogy of Martian low-albedo regions from MGS-TES data: Implications for upper crustal evolution and surface alteration

A. Deanne Rogers[1] and Philip R. Christensen[2]

Received 4 April 2006; revised 12 August 2006; accepted 30 August 2006; published 13 January 2007.

[1] Mars Global Surveyor Thermal Emission Spectrometer (MGS-TES) data are used to derive the modal mineralogy of spectrally distinct Martian low-albedo regions and to identify spatial trends in mineralogic assemblages. Results from this work are consistent with the major results of previous spectroscopic studies: (1) Plagioclase and clinopyroxene are the dominant minerals of most southern highlands regions, (2) the northern plains exhibit the lowest pyroxene abundance within Martian low-albedo regions, and (3) the highest concentrations of high-silica phase(s) are found in the northern plains, Solis Planum and a few southern high-latitude regions. Low-albedo regions may be classified into four units on the basis of relative abundances of plagioclase, pyroxene, and high-silica phase(s). Unit distributions between ±45° latitude exhibit moderate correlation with distinct provinces (e.g., Syrtis Major, Aonium Sinus) defined by large-scale morphology, elevation, and to some extent, surface age, suggesting that the spectral and compositional differences between these units are more strongly controlled by original bedrock mineralogy than by surface-atmosphere interactions and alteration. Syrtis Major exhibits a difference in mineralogy from the surrounding highlands suggesting a differing degree of fractional crystallization, assimilation, or source region composition. Areas with thick crust near the Tharsis Plateau exhibit lower abundances of olivine and greater plagioclase/pyroxene ratios than surrounding highland terrains, suggesting that magmas in this region may have undergone increased olivine fractionation. Regions where surface alteration is more likely to be the primary control on observed spectral signatures are the high-latitude areas (>45°), where globally, surfaces dominated by high-silica phase(s) are most commonly found.

Citation: Rogers, A. D., and P. R. Christensen (2007), Surface mineralogy of Martian low-albedo regions from MGS-TES data: Implications for upper crustal evolution and surface alteration, *J. Geophys. Res.*, *112*, E01003, doi:10.1029/2006JE002727.

1. Introduction

[2] One of the primary goals of acquiring spectroscopic observations of Mars is to determine surface mineralogy. Understanding surface mineralogy is important because (1) it can be a record of hydrothermal activity and past climatic conditions, and (2) the composition of the planet interior, and the degree of variation in magma compositions may be inferred.

[3] A companion paper [*Rogers et al.*, 2007] (hereinafter referred to as Paper 1) demonstrated that subtle, but spatially coherent infrared spectral differences exist between some Martian low-albedo regions. On the basis of the conclusions reached in Paper 1 that the spectral differences are likely due to spatial variations in mineralogy (primary and/or secondary phases), in this work we derive the mineralogy for spectrally distinct low-albedo regions and investigate the implications of the observed variations. Representative spectra from the low-albedo regions are grouped according to similar composition. The spatial distributions of these compositions are examined in the context of surface age, crustal terranes, elevation and latitude.

[4] Geologic context is useful where deciphering aspects of a region's geologic history from mineralogical information. However, even with context it is a challenge to relate the observed geologic record (preserved through stratigraphic relationships in composition and morphology) to the evolution of the Martian interior or alteration history. For example, much of the Noachian crust has probably been redistributed by meteorite impacts [e.g., *Strom et al.*, 1992; *Zuber*, 2001], and possibly also undergone mineralogical alteration due to impact-related shock [e.g., *McSween*, 1994; *Stöffler and Langenhorst*, 1994; *Grieve et al.*, 1996; *Johnson et al.*, 2002; *Strom et al.*, 1992; *Wright et al.*, 2004; *Johnson et al.*, 2006]. Second, nearly all surfaces as observed from orbit are covered by loose particulate sediments, at the spatial resolution of the TES instrument (~3 × 8 km) [*Christensen et al.*, 2001]. Although it is likely that surface rocks and sand are at least regionally

[1]Division of Geological and Planetary Sciences, California Institute of Technology, Pasadena, California, USA.
[2]Department of Geological Sciences, Arizona State University, Tempe, Arizona, USA.

0148-0227/07/2006JE002727$09.00

derived (within several hundred km) [e.g., *Edgett and Christensen*, 1991; *Greeley and Kraft*, 2001; *Rogers and Christensen*, 2003], the actual distance they have been transported from their igneous or sedimentary source, and the fluid (wind or water) in which they were transported may be unknown. Third, there is strong evidence for past hydrothermal activity, standing bodies of water, and groundwater sapping and/or short-lived precipitation on the surface [e.g., *Sharp and Malin*, 1975; *Carr*, 1996; *Aharonson et al.*, 2002; *Hynek and Phillips*, 2003; *Christensen and Ruff*, 2004; *Mangold et al.*, 2004; *Squyres et al.*, 2004; *Glotch and Christensen*, 2005; *Howard et al.*, 2005; *Irwin et al.*, 2005]; these events are another source for physical and/or chemical crust modification. Fourth, surface alteration may affect the relative abundances of primary minerals [*Colman*, 1982; *Eggleton et al.*, 1987; *Michalski et al.*, 2004; *Hurowitz et al.*, 2005; *McAdam et al.*, 2006]. Therefore observed abundances could be misinterpreted as reflecting original igneous mineralogy [e.g., *Michalski et al.*, 2004]. Fifth, primary high-silica volcanic glasses are potentially indistinguishable from some secondary amorphous or poorly crystalline high-silica materials in the thermal infrared spectral region [*Bandfield*, 2002; *Wyatt and McSween*, 2002; *Kraft et al.*, 2003; *Michalski et al.*, 2003; *Morris et al.*, 2003; *Ruff*, 2004; *Koeppen and Hamilton*, 2005], which complicates interpretation of high-silica phase(s) detected by the TES instrument. Finally, thermal infrared observations are only sensitive to the upper tens of microns of surface materials, leaving open the possibility that the remaining upper crustal materials have a different composition [e.g., *Hamilton et al.*, 2003a]. Because of these complicating factors, spatial distributions in mineralogy cannot always be unequivocally attributed to a certain process or sequence of events. However, in some areas, the combined evidence from mineralogy and geomorphology convincingly record magmatic evolution (e.g., basalts and dacites in Nili Patera [*Christensen et al.*, 2005]) or aqueous processes (e.g., hematite-bearing units in Meridiani Planum and Aram Chaos deposited in water-rich environments [*Christensen and Ruff*, 2004; *Glotch and Christensen*, 2005]). In this work, multiple interpretations of the results are presented, with identification of the most likely interpretation where possible.

2. Background

2.1. Remote Spectroscopic Observations

[5] Visible/near-infrared (VIS/NIR) and thermal infrared (TIR) remote spectroscopic observations have revealed much information about the mineralogy of the Martian surface (see reviews and summaries by *Singer et al.* [1979], *Soderblom* [1992], *Roush et al.* [1993], *Christensen et al.* [2001], *Bibring et al.* [2005], and *Christensen et al.* [2005]). On regional and global scales, pyroxenes, plagioclase, and high-silica phase(s) dominate the mineralogy of low-albedo regions. Pyroxene has been identified as a major component in Martian low-albedo regions with both VIS/NIR and TIR observations [*Adams and McCord*, 1969; *Singer and Roush*, 1985; *Bibring et al.*, 1990; *Mustard et al.*, 1993; *Bell et al.*, 1997; *Moersch et al.*, 1997; *Bandfield et al.*, 2000; *Christensen et al.*, 2000a; *Hamilton et al.*, 2001; *Bandfield*, 2002]. The presence of both high-Ca and low-Ca pyroxenes were reported using Phobos II Imaging Spectrometer for Mars (ISM) and Mars Express Observatoire pour la Mineralogie, l'Eau, les Glaces, et l'Activite (OMEGA) observations [*Mustard and Sunshine*, 1995; *Mustard et al.*, 1997; *Bibring et al.*, 2005; *Mustard et al.*, 2005]. Low-Ca pyroxene is identified across broad areas (several hundred km^2 in area) in the cratered highlands, however, the relative abundance of high-Ca pyroxene is always greater than low-Ca pyroxene (ratios range from 80:20 to 60:40) [*Mustard et al.*, 2005]. Plagioclase is another major component of Martian low-albedo regions [*Bandfield et al.*, 2000; *Christensen et al.*, 2000a; *Hamilton et al.*, 2001; *Bandfield*, 2002], and is usually more abundant than pyroxene [*Hamilton et al.*, 2003a]. Finally, "high-silica" (meaning Si/O > ~0.35 [after *Michalski et al.*, 2005a]) amorphous or poorly crystalline phase(s) are found in most low-albedo regions at abundances of 15–20%; higher abundances are found in the north polar dunes, Acidalia Planitia, Solis Planum, and a few low-albedo areas in the southern highlands [*Bandfield*, 2002; *Bandfield et al.*, 2002; *Aben*, 2003]. This high-silica component may be interpreted as primary volcanic glass [*Bandfield et al.*, 2000; *Hamilton et al.*, 2001, 2003b], zeolites [*Ruff*, 2004], amorphous silica coatings [*Wyatt and McSween*, 2002; *Kraft et al.*, 2003; *McLennan*, 2003; *Minitti et al.*, 2003, 2005] and/or poorly crystalline material in weathering rinds [*Kraft et al.*, 2005; *Michalski et al.*, 2005b]. In addition to amorphous silica, *Wyatt and McSween* [2002] also suggested phyllosilicates as possible candidates for the observed high-silica component, but lab studies and further TES data analyses have shown that phyllosilicates are less likely. Those interpretations are based on (1) differences between fundamental absorption positions of the TES high-silica phase(s) and those of phyllosilicates measured in the laboratory [*Koeppen and Hamilton*, 2005; *Michalski et al.*, 2005a], and (2) lack of evidence for both the 465 and 530 cm^{-1} absorptions associated with dioctahedral phyllosilicates in TES data [*Ruff*, 2003]. VIS/NIR spectra also do not show significant phyllosilicate absorptions in low-albedo regions [e.g., *Soderblom*, 1992; *Blaney et al.*, 2003; *Bibring et al.*, 2005], providing further evidence against a phyllosilicate origin for the TES high-silica phase(s).

[6] Global-scale differences in thermal infrared spectral properties were identified by *Bandfield et al.* [2000]. Thermal emission spectra from low-albedo regions were classified into three groups: (1) Surface Type 1, which is generally concentrated in the southern highlands [*Bandfield et al.*, 2000], with a few isolated exceptions in the northern lowlands [*Rogers and Christensen*, 2003], (2) Surface Type 2, which is primarily located in the northern lowlands but also has significant concentrations scattered throughout the southern highlands [*Bandfield et al.*, 2000], and (3) a spectral shape that is intermediate between, and can be modeled as a mixture of, the two surface types. The Surface Type 1 spectral shape has been interpreted as basalt [*Bandfield et al.*, 2000; *Christensen et al.*, 2000a; *Hamilton et al.*, 2001; *Wyatt and McSween*, 2002] and Surface Type 2 has been interpreted as basaltic andesite [*Bandfield et al.*, 2000; *Hamilton et al.*, 2001] or basalt plus a secondary high-silica amorphous or poorly crystalline phase [*Wyatt and McSween*, 2002; *Kraft et al.*, 2003; *Morris et al.*, 2003; *Wyatt et al.*, 2004; *Michalski et al.*, 2005a].

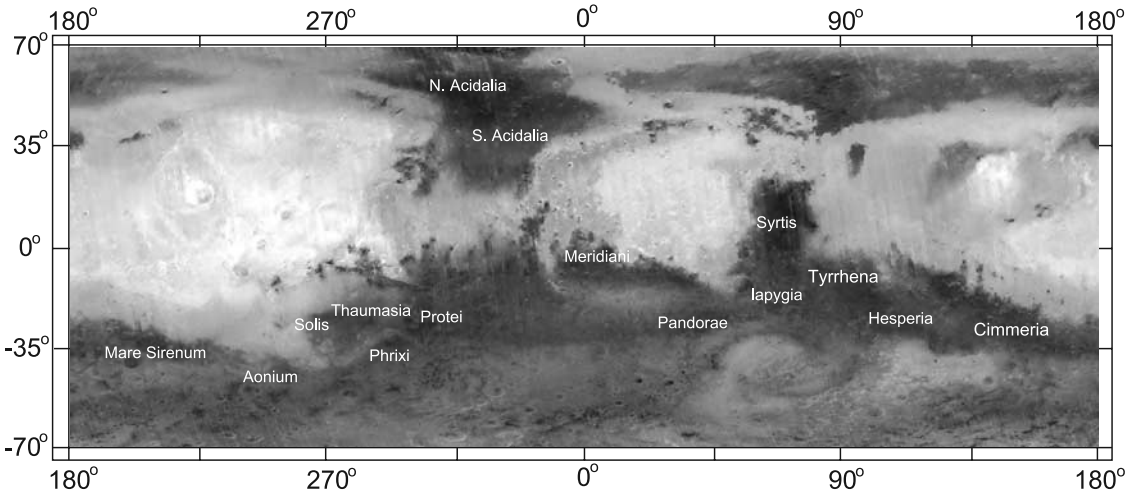

Figure 1. Names and locations of geographic areas discussed in this work. The background image is TES albedo [*Christensen et al.*, 2001]. The albedo range shown is 0.07 (darkest tones) to 0.35 (lightest tones).

[7] Local-scale enrichments of high-Ca clinopyroxene, low-Ca pyroxene, and olivine have been mapped with both TIR and VIS/NIR data sets [*Christensen et al.*, 2003; *Hamilton et al.*, 2003a; *Hoefen et al.*, 2003; *Hamilton*, 2004; *Bibring et al.*, 2005; *Christensen et al.*, 2005; *Hamilton and Christensen*, 2005; *Mustard et al.*, 2005; *Rogers et al.*, 2005]. Outcrops enriched in low-Ca pyroxene are limited to Noachian terrains, whereas high-Ca pyroxene and olivine-enriched regions are found in a wider range of age units [*Bibring et al.*, 2005; *Mustard et al.*, 2005]. Finally, local enrichments of phyllosilicates [*Bibring et al.*, 2005; *Poulet et al.*, 2005], sulfates [*Arvidson et al.*, 2005; *Gendrin et al.*, 2005], quartz/feldspars [*Bandfield et al.*, 2004; *Christensen et al.*, 2005; *Hamilton*, 2005] and gray crystalline hematite [*Christensen et al.*, 2000b; *Knudson and Christensen*, 2004; *Glotch and Christensen*, 2005; *Glotch et al.*, 2005] have also been identified.

[8] These complementary spectroscopic observations provide constraints on the degree to which Martian meteorite lithologies are representative of the Martian surface [e.g., *Hamilton et al.*, 2003a]. Shergottites typically contain both low-Ca and high-Ca pyroxenes. Proportions of these two pyroxenes have not been reported for all shergottites, but those with measured modal abundances have proportions that range from ~1:1 to ~18:1 [e.g., *Stolper and McSween*, 1979; *McSween and Jarosewich*, 1983; *Treiman et al.*, 1994; *Hale et al.*, 1999; *Zipfel et al.*, 2000; *Barrat et al.*, 2002; *Taylor et al.*, 2002; *Goodrich*, 2003]. OMEGA data reveal that some areas exhibit low-Ca and high-Ca pyroxene proportions of 40:60 [*Mustard et al.*, 2005], which is approaching but not within the measured shergottite range listed above. Usually, the proportion of low-Ca pyroxene is much less than that of high-Ca pyroxene [*Hamilton et al.*, 2003a; *Mustard et al.*, 2005]. In addition, TIR spectra and derived plagioclase/pyroxene ratios from most low-albedo regions do not match the majority of the Martian meteorites [*Bandfield et al.*, 2000; *Christensen et al.*, 2000a; *Christensen et al.*, 2001; *Hamilton et al.*, 2003a]. Finally, TES-derived Mg/Al and Al/Si ratios from Surface Type 1, which spans Noachian and Hesperian terrains, are more similar to terrestrial basalts than to the Martian meteorites [*McSween et al.*, 2003]. Therefore the basaltic Martian meteorites and their characteristic total pyroxene abundances are probably not representative of the bulk composition of the Martian crust [*Bandfield et al.*, 2000; *Hamilton et al.*, 2003a; *McSween et al.*, 2003]. The Martian meteorites (except for ALH84001) may instead represent younger plume magmatism that was chemically different than the ancient crust [*McSween et al.*, 2003, 2004].

2.2. Global-Scale Spectral Variability

[9] Conclusions from both VIS/NIR and TIR spectral studies suggest that, with the exception of many local-scale enrichments of various mineral types [*Christensen et al.*, 2003; *Hamilton et al.*, 2003a; *Hoefen et al.*, 2003; *Christensen et al.*, 2005; *Bibring et al.*, 2005; *Gendrin et al.*, 2005; *Hamilton and Christensen*, 2005; *Mustard et al.*, 2005; *Rogers et al.*, 2005; *Martinez-Alonso et al.*, 2006], low-albedo regions are generally homogeneous on a regional scale but vary in mineralogy from region-to-region [e.g., *Erard et al.*, 1991; *Mustard et al.*, 1997; *Bandfield et al.*, 2000; *Bandfield*, 2002; *Rogers et al.*, 2007]. Recent results from the Gamma Ray Spectrometer (GRS) also suggest regional crustal differences in elemental composition [*Taylor et al.*, 2006]. In this work, we use additional spectral detail extracted from the TES data set (Paper 1) to present new and refined compositional units and their distributions. The distributions and derived mineralogy are used to discuss implications for surface alteration and development of the crust. New consideration of the nature and aspects of Surface Type 2 [*Bandfield et al.*, 2000] is included in the discussion.

3. Approach

[10] The approach in this work is different than previous TIR global composition studies [e.g., *Bandfield*, 2002, 2003] in that we address region-to-region differences in modal mineralogy. Spatial distributions of mineralogic

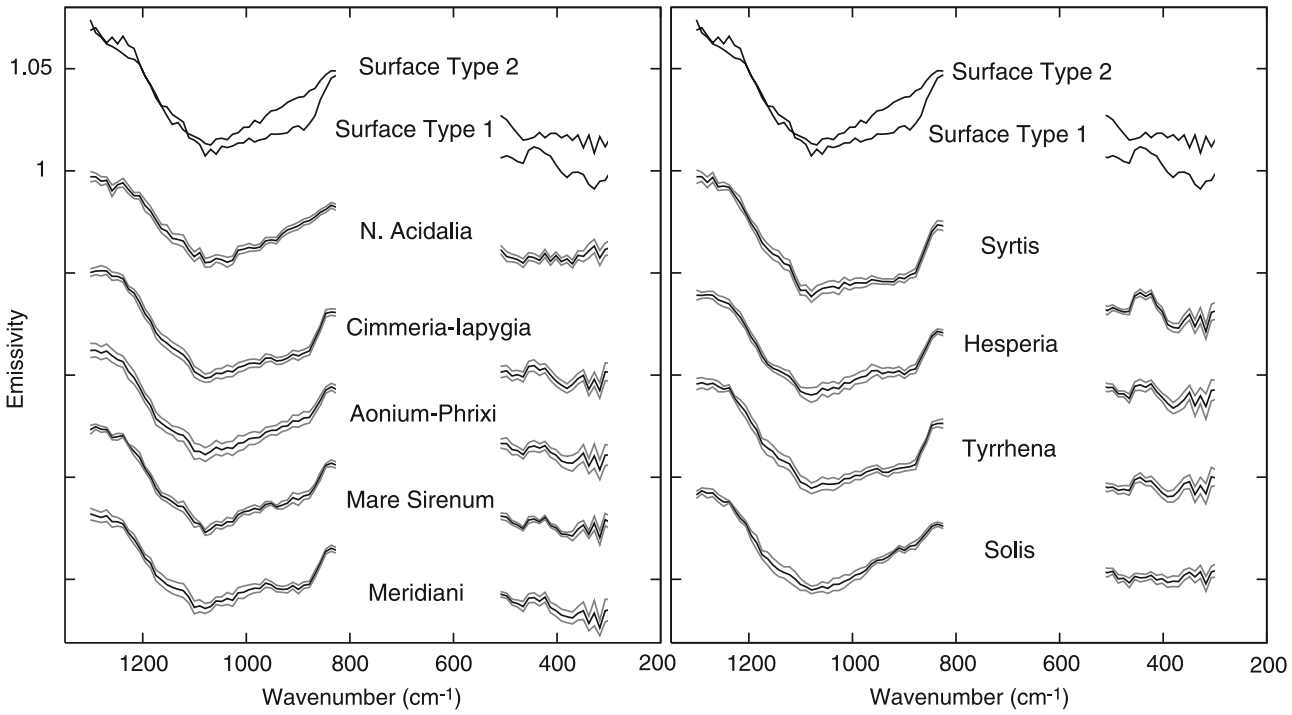

Figure 2. Representative spectral shapes from Paper 1, for which modal mineralogy is derived using linear deconvolution [*Ramsey and Christensen*, 1998]. Thin lines indicate the standard deviation for each spectrum.

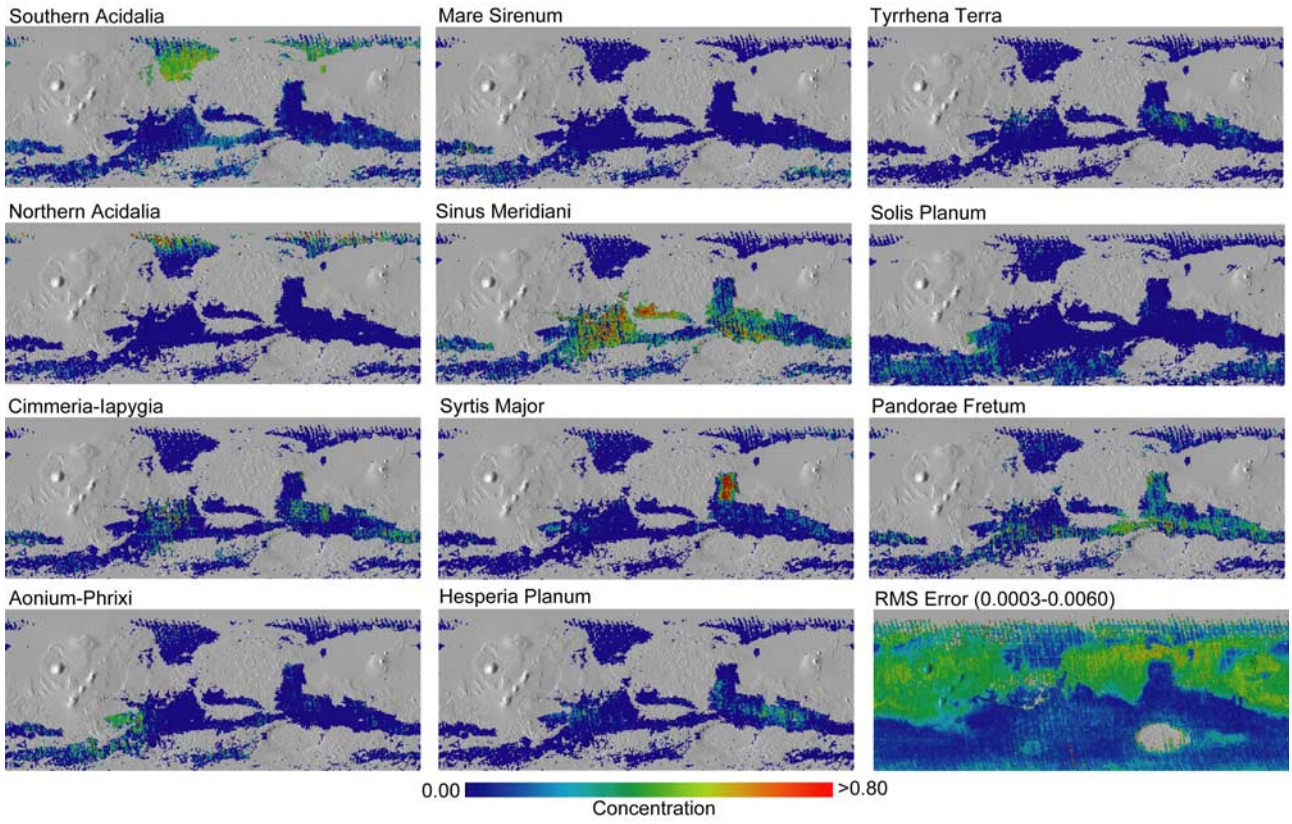

Figure 3. Distributions of spectral shape concentrations from Paper 1.

assemblages, rather than a single mineral group, are examined in an effort to understand their relationship to crustal evolution and alteration. This paper contains references to various age and crustal terranes. A map of geographic locations discussed in this work is provided in Figure 1. Additionally, the terms "region"/"regional" and "local-scale" are used throughout this paper. In this work, these terms generally refer to areas on the order of $\sim 10^4$ to 10^6 km^2 and $\sim 10^1$ to 10^3 km^2, respectively.

[11] Spectral differences between large, low-albedo regions are first determined (Paper 1), and then modal mineralogy is derived for each spectrally different region. Using this method, a regionally dominant modal mineralogy may be derived, and global trends in the distribution of mineralogic assemblages can be better visualized. The potential disadvantages are that (1) pixels that are modeled as mixtures of these spectral shapes can be difficult to interpret and that (2) local-scale enrichments in a single mineral group may be obscured. However, locating small-scale mineral concentrations is not the purpose of this study. Finally, spectral differences between each representative shape are subtle (Paper 1), therefore the derived mineralogy for one shape will not necessarily be statistically unique from all other shapes. The spectral shapes (Figure 2) are grouped into compositional units by similarity in derived bulk mineralogy, and the global distribution of each compositional unit is determined by summing the concentration maps (Figure 3, derived in Paper 1) for each representative shape that is part of that unit.

[12] Eleven spectral shapes representative of Martian low-albedo regions were derived in a companion paper using TES data (Paper 1). One of these, the southern Acidalia representative shape, may be influenced by thin dust coatings (Paper 1). It would be inappropriate to use a linear combination of coarse-particulate mineral spectra to model spectral features that may be due to dust coatings, therefore a modal mineralogy for that spectral shape is not derived in this work. In addition, a lower confidence level was afforded to a second spectral shape, found primarily in the Pandorae Fretum region (Paper 1). The Pandorae spectral shape is also excluded.

[13] Modal mineralogy associated with each of the nine remaining spectral shapes (Figure 2) is derived using the linear deconvolution method [*Ramsey and Christensen*, 1998], from 307–1301 cm^{-1}. In this method, a library of 47 potential spectral end-members (Table 1) is used to fit the TES-derived spectral shape in an linear least squares fashion, whereby spectra used in negative (and therefore geologically meaningless) concentrations are iteratively removed from the set until only library spectra with positive concentrations remain in the solution. Using this method, it is possible that a correct low-abundance end-member may be ejected from the solution [*Bandfield et al.*, 2000; *Seelos and Arvidson*, 2003]; however, in practice, this rarely occurs [e.g., *Feely and Christensen*, 1999; *Hamilton and Christensen*, 2000; *Seelos and Arvidson*, 2003]. One indication that a correct end-member may have been dropped is if the RMS error decreases upon lowering the number of library spectra allowed in the model. In this work, we evaluate the numerical uncertainty associated with the modeled abundances of the major components from this technique using three different methods.

Table 1. Spectral Library[a]

Mineral Group	End-Member
Quartz	Quartz BUR-4120
Feldspar	Microcline BUR-3460
	Orthoclase WAR-RGSAN01(a)
	Albite WAR-0244
	Oligoclase WAR-5804
	Andesine BUR-240
	Labradorite WAR-4524
	Bytownite WAR-1384
	Anorthite BUR-340
	Shocked An 22.6 Gpa(b)
	Shocked An 56.3 GPa(b)
Orthopyroxene	**Bronzite NMNH-93527**
	Enstatite HS-9.4B
	Bronzite BUR-1920
Clinopyroxene	**Diopside WAR-6474**
	Augite NMNH-9780(c)
	Augite NMHN-122302(c)
	Hedenbergite manganoan DSM-HED01
	Pigeonite(c)
Olivine	**Forsterite BUR-3720A**
	Fayalite WAR-RGFAY01
	KI 3115 Fo68(d)
	KI 3362 Fo60(d)
	KI 3373 Fo35(d)
	KI 3008 Fo10(d)
Zeolite	crystalline heulandite(e)
	crystalline stilbite(e)
Sheet-silicates	**Biotite BUR-840**
	Muscovite WAR-5474
	Serpentine HS-8.4B
	Antigorite NMNH-47108
	Illite granular IMt-2 minus 60%bb[b]
	Ca-montmorillonite solid STx-1
	saponite<0.2 mic plus 60%bb(f)[b]
Amorphous silica	**K-rich Glass(g)**
	SiO2 Glass(g)
	opal-A (01-011)(h)
	Al-Opal(i)
Amphibole	**Magnesiohastingsite HS-115.4B**
	Actinolite HS-116.4B
	Magnesiohornblende WAR-0354
Hematite	**Average Martian Hematite(j)**
Carbonate	**Calcite C40**
	Dolomite C20
Sulfate	**Anhydrite ML-S9**
	Gypsum ML-S6
Surface dust	average high-albedo surface(k)
Blackbody	**blackbody**

[a]Mineral spectra are from the ASU spectral library available online at http://tes.asu.edu [*Christensen et al.*, 2000c], with the following exceptions, denoted by letters in parentheses after entries: (a) provided by S. W. Ruff, samples described by *Ruff* [1998]; (b) *Johnson et al.* [2002]; (c) provided by V. E. Hamilton, described by *Hamilton* [2000]; (d) provided by V. E. Hamilton, samples described by *Morse* [1996]; (e) described by *Ruff* [2004]; (f) described by *Michalski et al.* [2005a]; (g) described by *Wyatt et al.* [2001]; (h) described by *Michalski et al.* [2003]; (i) provided by M. D. Kraft (personal communication, 2005); (j) derived from TES data, described by *Glotch et al.* [2004]; and (k) derived from emission phase function observations with TES by *Bandfield and Smith* [2003]. Bold text designates end-members that comprise the skeleton library. See text for details.

[b]Spectrum was scaled to produce comparable spectral contrast to that of other solid clays in the ASU library. See text for details.

[14] First, phases that were typically modeled in low abundance (<5%), but above zero, were alternately excluded from the library set, to evaluate the influence of these minor components on the derived abundances of the dominant phases. These minor components are quartz, amphiboles, and orthoclase. In addition, it was found that the presence/absence

Table 2. Derived Modal Mineralogy[a]

	Syrtis		Tyrrhena		Cimmeria-Iapygia		Aonium-Phrixi		Hesperia		Mare Sirenum		Meridiani[b]		Solis		N. Acidalia	
Plagioclase[c]	31	*2*	24	*1*	27	*2*	38	*4*	24	*2*	33	*3*	24	*2*	29	*4*	32	*1*
Alkali Feldspar	1	*3*	2	*4*	1	*1*	0	*1*	0	*0*	0	*0*	1	*2*	2	*2*	0	*0*
High-Ca Clinopyroxene	29	*1*	20	*4*	19	*2*	20	*2*	20	*1*	20	*1*	22	*2*	6	*2*	7	*2*
Orthopyroxene	4	*2*	6	*1*	7	*1*	6	*1*	5	*1*	6	*1*	3	*0*	14	*1*	16	*2*
Pigeonite	0	*0*	8	*5*	6	*3*	0	*0*	5	*3*	1	*1*	0	*0*	1	*3*	0	*0*
Olivine	7	*1*	12	*1*	11	*1*	3	*1*	11	*1*	5	*0*	11	*0*	6	*1*	1	*1*
Carbonate	7	*0*	4	*0*	5	*0*	6	*0*	5	*0*	5	*0*	6	*0*	2	*0*	4	*0*
Sulfate	3	*2*	7	*1*	6	*1*	6	*0*	9	*0*	7	*0*	8	*0*	7	*1*	6	*0*
High-silica phase(s)	12	*3*	13	*2*	16	*3*	17	*2*	19	*1*	21	*2*	22	*4*	31	*4*	34	*2*
Amphibole	3	*2*	2	*1*	1	*1*	2	*1*	0	*0*	0	*0*	0	*0*	0	*0*	1	*1*
Hematite	0	*0*	0	*0*	0	*0*	0	*0*	0	*0*	0	*0*	0	*0*	0	*0*	0	*0*
Quartz	2	*1*	1	*1*	2	*1*	2	*1*	0	*0*	2	*1*	2	*0*	1	*1*	0	*0*
Plagioclase/pyroxene	0.9		0.7		0.8		1.5		0.8		1.3		1.0		1.4		1.4	
RMS error low,[d]%	0.152		0.114		0.122		0.127		0.134		0.127		0.123		0.110		0.136	
RMS error high,[d]%	0.181		0.126		0.139		0.149		0.139		0.145		0.127		0.123		0.139	

[a]Values are percent. Italics indicate $\pm 1\sigma$ for derived abundances.
[b]Average, standard deviation and RMS errors are derived from a subset of the five model results. See text for explanation.
[c]"Plagioclase" group includes shocked plagioclase endmembers.

of pigeonite in some cases affected the modeled abundance of other phases in a similar manner to orthoclase, therefore we also evaluated the influence of pigeonite on the final derived mineralogy. Model results from each of the five library variations were examined to ensure that there were (1) no significant changes in the derived abundance of the major components, and (2) no decrease in RMS error where one of these minor phases was excluded from the library set. Neither of these effects were observed for eight of the nine spectral shapes. In those cases, results from the five models using the standard library were averaged and reported with one standard deviation (Table 2). These deviations give a sense of the range of abundances observed where these minor phases were excluded. For the Meridiani spectral shape, however, two model results were dropped before averaging. This is discussed in more detail in section 4.1. The advantage of this approach to mineral abundance estimation is that the major components are derived from an average of multiple model attempts, which avoids a bias in mineralogical results that might arise from using only one spectral library. A consequence is that the abundances of small components (e.g., quartz and amphiboles) will be decreased.

[15] Second, a skeleton library consisting of a minimum amount of spectra to account for all major igneous and alteration mineral types (24 spectra), was compiled for use. The skeleton library was used to corroborate the major phase abundances derived from the standard library runs, but was not used in the final average. Abundances derived using the skeleton library matched those derived using the full library to better than 5% for the major components (plagioclase, high-Ca clinopyroxene, low-Ca pyroxene, olivine, and high-silica phases), with two exceptions: (1) the Meridiani shape was modeled with 10% more high-silica phases using the skeleton library, and (2) the Tyrrhena shape was modeled with 10% more plagioclase using the skeleton library. The Meridiani shape is discussed further in section 4.1. For Tyrrhena Terra, the modal abundances derived from the skeleton library are adversely affected by the lack of olivine spectra present in that library. This was evident from examining the derived mineralogy using the full library; the model results included olivine spectra that were not present in the skeleton library.

[16] One last check on the derived mineralogy comes from least-squares fitting with nonnegativity constraints [*Lawson and Hanson*, 1974]. This technique differs from *Ramsey and Christensen* [1998] in that all potential endmembers are kept in the design matrix while the algorithm finds the nonnegative coefficients for each spectrum that provide the best fit to the mixed spectrum. A similar approach was applied to deconvolution of TES data by *Seelos and Arvidson* [2003]. The benefit is that the possible, though rare [*Feely and Christensen*, 1999; *Bandfield et al.*, 2000; *Hamilton and Christensen*, 2000] effect of a correct end-member being dropped in the iterative process is avoided. To be consistent with previous studies, the derived mineralogy using the method of *Ramsey and Christensen* [1998] as described above is reported in Table 2; however, the least-squares fitting method of *Lawson and Hanson* [1974] is used to corroborate the final derived mineralogy and classification. In applying this method, we found that the abundance of all phases for all spectral shapes agreed to within 5% of the iterative method, with two exceptions: (1) the model result for the Meridiani shape yields 9% low-Ca pyroxene abundance (as opposed to 3% with the iterative method), and (2) Solis Planum high-silica phase abundance is lower than iterative models by 6%.

[17] Finally, notes about the source of each spectrum in our library are listed in the footnotes of Table 1, however here we provide more detail about the illite and saponite spectra used. The only available illite spectrum in the ASU library was collected from a "granular" sample, meaning gravel-sized particles broken from "solid" samples [*Piatek*, 1997]. "Solid" clay samples in the ASU library were prepared by mixing silt-sized clay powders with water, forming the mixture into 2 cm diameter discs, and allowing the samples to dry at room temperature for approximately one week [*Piatek*, 1997]. The actual particle sizes of the

granular samples, though generally labeled as "gravel"-sized, were not measured and could have varied between and within individual samples. Thus the spectra from solid clay disc samples are preferred over the granular samples when available, because any differences in spectral feature depth between the granular forms of each of the available clay samples could be due to physical effects, as opposed to natural spectral contrast differences. Conversely, the best available saponite spectrum is from a pressed pellet of <0.2 micron particles [*Michalski et al.*, 2005a], which exhibits a spectral contrast much deeper than the average contrast of the solid samples. If phyllosilicates exist in Martian low-albedo regions, plausible forms could range from coarse grained particles to rock coatings [*Michalski et al.*, 2005a], meaning that the spectral contrast of either the "granular", "solid", or pressed pellet samples could be appropriate. The solid samples are intermediate in contrast between these three options. To avoid overestimating or underestimating the relative abundance of illite and saponite relative to other phyllosilicates and primary minerals in our library, we chose to scale the illite and saponite spectra to match the average spectral contrast of solid clays in the ASU library. Adjusting the contrast has no influence on which minerals are ultimately chosen in the best fit solution during deconvolution. However, it is possible that the actual clay abundances could be misrepresented if clays on the Martian surface have a spectral contrast much lower or higher than the average solid clays in the ASU library. In this work, phyllosilicates were typically modeled in abundances of less than 5%; inappropriate scaling of these end-members would result in a maximum absolute error of 3%. For Solis Planum and N. Acidalia, phyllosilicates were modeled in abundances between 10 and 15%; in these cases the maximum absolute error from inappropriate scaling is 6–9%.

4. Results

4.1. Derived Mineralogy

[18] Derived mineralogy for each spectral shape (Figure 2) is given in Table 2. For the Meridiani spectral shape, two model results were dropped from the average—those derived using the full library and those from the quartz-excluded library. RMS errors actually improve if either pigeonite, orthoclase, or amphiboles are excluded from the full library (errors of 0.127%, 0.124%, 0.123%, respectively vs. 0.151% for the full library). In addition, orthoclase abundance using the full library was 15% greater than that of the other models. Finally, the RMS error using the skeleton library was slightly lower than that of the full library (0.145% versus 0.151%), further indicating that the results using the full library were suspect. The model fit noticeably worsened with the quartz-excluded library (RMS errors of 0.180%) and produced similar mineralogical results to the full library, therefore it was also excluded from the average.

[19] In general, plagioclase, high-Ca clinopyroxene, and high-silica phase(s) are the dominant mineral groups for most regions (Table 2). Additional mineral groups are modeled at or below the detection limit for normalized abundances (~5–15%, depending on the mineral group [*Christensen et al.*, 2000a, 2001]), including orthopyroxene, olivine, pigeonite, carbonate, sulfate, and amphibole (Table 2). The average mineralogy determined for these regional surface emissivity shapes (Table 2) may reflect either a homogeneous surface composition for that region, or a mixture of the regional composition with abundant local-scale outcrops that are enriched in a particular mineral group, such as olivine.

[20] A new result of this work is that some regions exhibit equal abundances of plagioclase and total pyroxene, and in some areas, total pyroxene abundance exceeds plagioclase abundance (Table 2). This result was not recognized in previous studies because high- and low-Ca pyroxene abundances were not summed. However, after revisiting the mineral maps of *Bandfield* [2002], it was found that those maps also show areas with greater total pyroxene abundance, in agreement with this study. Thus plagioclase does not always dominate the mineralogy of all low-albedo regions; however, it is rarely present at significantly lower abundance than the total pyroxene fraction (Table 2).

[21] In some regions, low-Ca pyroxenes (orthopyroxene, pigeonite) and olivine are modeled at or above the traditional TES detection limits (Table 2). Additionally, modeled abundances of orthopyroxene and olivine differ by up to 13 and 11%, respectively, between regions (Table 2). These differences are also right at the standard detection limits. Because olivine and low-Ca pyroxene abundances are not well-above the detection limits, there may be some concern that using them to help classify the spectral units into mineralogical groups is questionable. However typically, if low-Ca pyroxene or olivine are modeled at a greater-than-average abundance, it is accompanied by a lower-than-average abundance of one of the major phases that is well above the detection limit, such as plagioclase. Thus low-Ca and olivine are never used as sole discriminators where classifying the spectral shapes into compositional groups. On a global scale, observations from OMEGA data show that low-Ca pyroxene is widely distributed in the Noachian highlands, although at lower abundances than high-Ca pyroxene [*Bibring et al.*, 2005; *Mustard et al.*, 2005]. The availability of supporting mineralogic data from OMEGA allows us to examine low-Ca pyroxene distributions, despite their low abundances relative to plagioclase, high-Ca pyroxene, and high-Si phase(s). Therefore, in this work, we explore observed mineralogic trends with these phases included.

4.2. Classification of Spectral Units by Mineralogy

[22] The spectral shapes were classified by their relative abundances of plagioclase, olivine, low-Ca pyroxene, high-Ca clinopyroxene, and high-silica phases. Sulfate, carbonate, amphibole, hematite, and quartz abundance vary by <6% between regions, and therefore are not used in spectral classification. A minimum-distance hierarchical clustering algorithm [e.g., *Anderberg*, 1973] was used to group the spectral shapes. Each spectral shape may be considered as a point in five-dimensional space whose coordinates are defined by its modal abundance of plagioclase, olivine, low-Ca pyroxene, high-Ca pyroxene, and high-silica phases. The algorithm calculates the distance between each of these points, and then merges the two closest points into a cluster. It then looks for the next two closest points, and merges them. If either of those two points were already in a cluster,

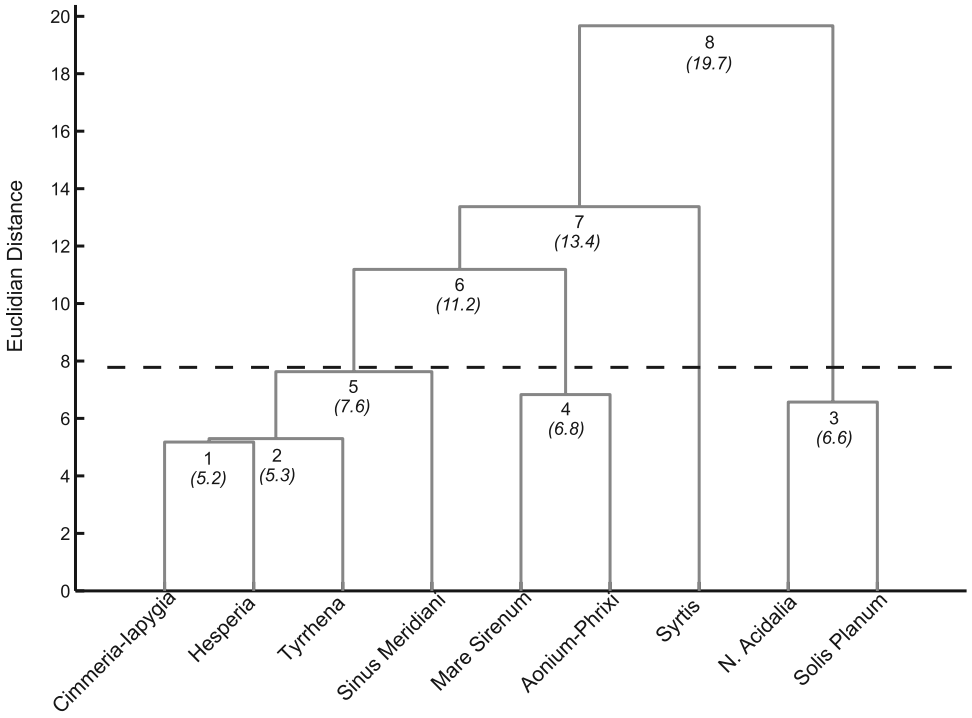

Figure 4. Dendrogram showing the results of the hierarchical clustering analysis. Each junction is numbered in order of merge step, and the distance between points at each merge step is given in parentheses. The dashed line designates the first natural break in minimum distance between points. Junctions below the dashed line form the four compositional groups discussed in this work. See section 4.2 for additional explanation.

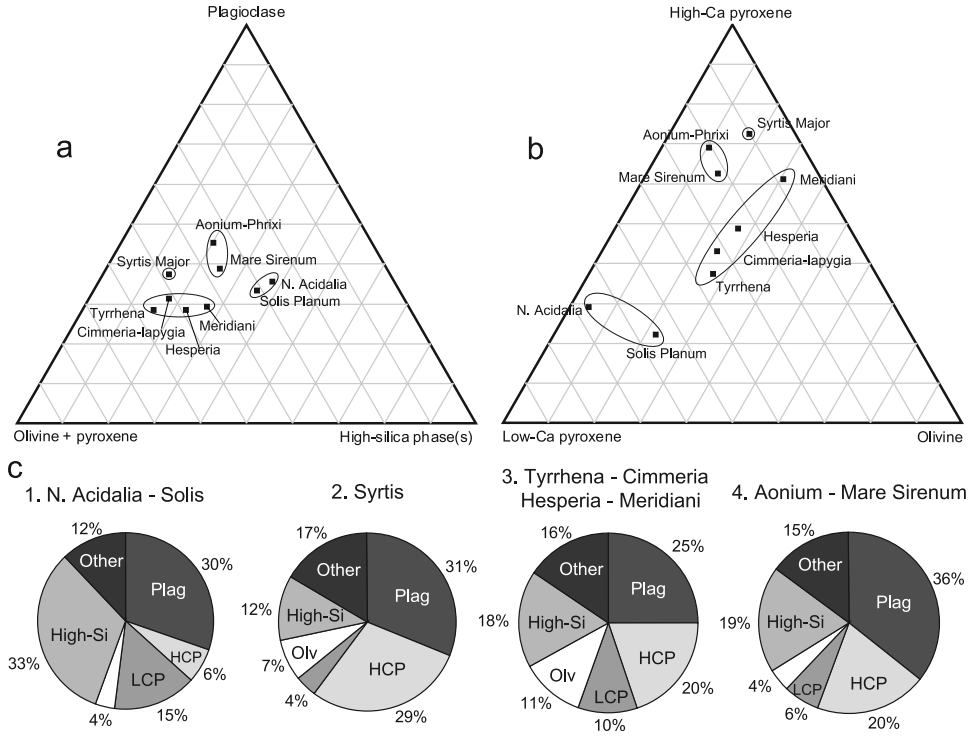

Figure 5. (a, b) Ternary diagrams used to display the modal mineralogy for each spectral shape. Note that the components are forced to sum to 100%; therefore the abundances are inflated from those shown in Table 2. The high-silica phase(s) group is the combined modeled abundance of phyllosilicates, glasses, and opals. (c) Pie charts showing the average derived mineral abundances for the spectral classes shown in Figures 4, 5a, and 5b. See section 4.2 for discussion of the Meridiani data point.

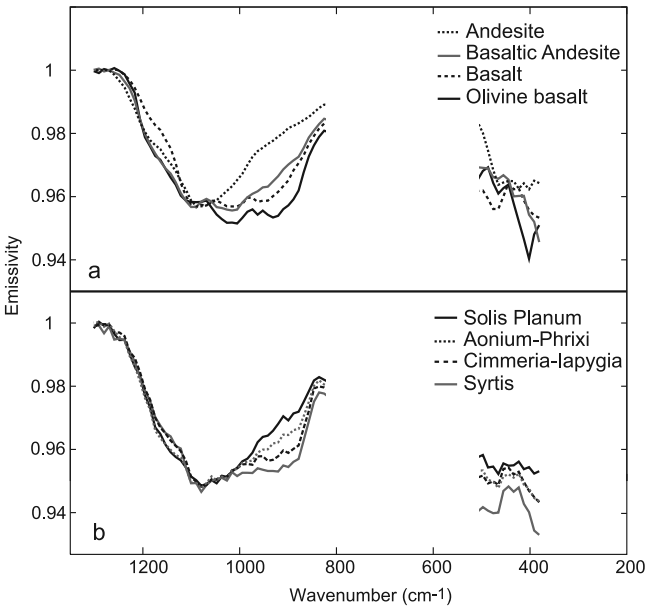

Figure 6. (a) Laboratory spectra of terrestrial volcanic rocks. (b) A representative spectral shape from each compositional group defined in section 4.2. Spectra are normalized to the same spectral contrast and offset for clarity. The spectral differences between each compositional group are subtle, but comparable to variation observed between mafic and intermediate volcanic rocks.

the stray point is added to the cluster. If neither point is already in a cluster, a new one is formed. The algorithm continues in this fashion until all points are in a single group. At each merge step, the algorithm returns the distance between the two points that were combined. Because all points eventually end up in the same group, the user must decide where to stop the merging of clusters. In this work, we simply used the first natural break in calculated minimum distance to halt the clustering (Figure 4). This resulted in a total of four clusters, or compositional groups.

[23] The four compositional groups are: (1) N. Acidalia + Solis Planum, (2) Syrtis Major, (3) Tyrrhena Terra + Hesperia Planum + Cimmeria-Iapygia + Meridiani, and (4) Aonium-Phrixi + Mare Sirenum. These classes may be visualized on a ternary diagram in Figure 5a, with the following mineral groups as vertices: plagioclase, ferromagnesian silicates (olivine + pyroxene), and high-silica phase(s). A second ternary diagram displaying high-Ca pyroxene, low-Ca pyroxene, and olivine on the vertices was also constructed (Figure 5b). The divisions from the clustering algorithm are evident in the mafic mineralogy as well, with the exception of Meridiani, which has a lower abundance of low-Ca pyroxene than the others in its group. Although the Meridiani spectral shape is modeled with a slightly lower low-Ca pyroxene abundance than the other spectral shapes in Group 3, there is reason to suggest that the Meridiani shape may in actuality have more low-Ca pyroxene than derived in Table 2 (3%). Model results from the skeleton library yield 7% low-Ca pyroxene abundance. In other cases where the skeleton library results showed greater low-Ca pyroxene abundance than the standard library, it was accompanied by a ~5–10% mismatch in olivine abundance. However, for the Meridiani spectral shape models, there is agreement to within 2% olivine between the standard and skeleton libraries. In addition, nonnegative least-squares fitting using the *Lawson and Hanson* [1974] method (section 3) indicates ~10% low-Ca pyroxene abundance. Finally, basaltic sands encountered by the Mars Exploration Rover Opportunity within Meridiani Planum contain ~10% low-Ca pyroxene [*Glotch and Bandfield*, 2006]. Spectra from the hematite unit in Meridiani Planum were not used in the "Sinus Meridiani" regional average shape (Paper 1); however, if it is assumed that the sands are similar to the surrounding Sinus Meridiani region, then this further suggests that perhaps the low-Ca pyroxene abundance in Table 2 is too low.

[24] The four compositional units are separated by ~10% or greater differences in plagioclase, high-Ca pyroxene, and high-silica phase(s). Differences of 10% or greater in olivine and low-Ca pyroxene abundance are also present between some groups. Group 1 consists primarily of high-silica phase(s) (~30–35%), plagioclase (~30%), and orthopyroxene (~15%). Group 2 surfaces consist primarily of high-Ca clinopyroxene (~30%), plagioclase (~30%), and high-silica phase(s) (~10%). Group 3 surfaces consist primarily of plagioclase (~25%), high-Ca clinopyroxene (~20%), high-silica phase(s) (~15–20%), low-Ca pyroxene (~5–15%), and olivine (~10–15%). Group 4 is characterized by ~35–40% plagioclase, ~20% high-Ca pyroxene, ~15–20% high-silica phase(s) and low (~5% or less) abundances of olivine and low-Ca pyroxene.

[25] These units cover the range of variability observed in the derived mineralogy for each representative spectral shape (Table 2). Although the spectral differences between these four groups are subtle, they are comparable to spectral variation associated with terrestrial mafic and intermediate volcanic rocks (Figure 6).

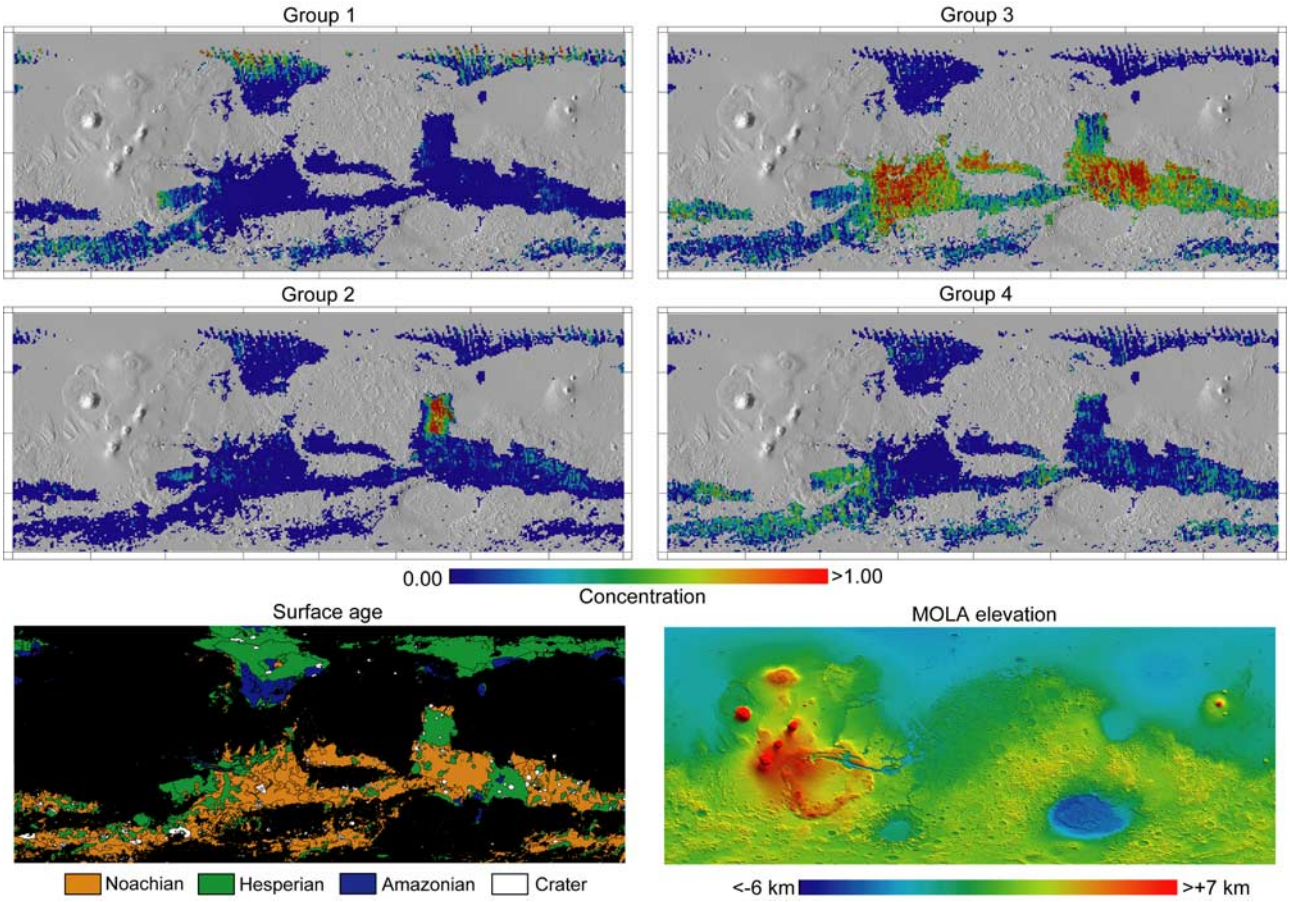

Figure 7. Maps of summed concentrations for each of the four compositional groups discussed in section 4.2 and shown in Figure 5. Each map covers the area −180°E to 180°E, 70°S to 70°N. Latitude ticks are spaced every 35°, and longitude ticks are spaced every 45°. Concentration values greater than 1.0 occur because the values represent the percentage of spectral feature depth of the nine spectral end-members. Some surfaces have greater spectral contrast than the end-members defined in Paper 1. For reference, a simplified age map [*Scott and Tanaka*, 1986; *Greeley and Guest*, 1987; *Tanaka and Scott*, 1987], color coded using the scheme of *Solomon et al.* [2005], and a MOLA elevation map are shown. Areas that are black or with no data have TES surface albedo values greater than 0.15 [*Christensen et al.*, 2001], with the exception of the Solis Planum region (24°S–35°S, 265°E–273°E) (refer to Paper 1). The southern Acidalia region has no concentration values because modal mineralogy was not derived for that region (section 3).

4.3. Distribution of Spectral Unit Classes

[26] Distributions for the spectral unit classes defined in Figure 4 are shown in Figure 7. Surfaces that exhibit albedo values >0.15 are masked out. One exception to this is the region between 24–35°S, 265–273°E (Solis Planum), which is masked on albedo values greater than 0.17 (Paper 1). Some pixels are modeled as a mixture of two or more spectral unit classes. For quantitative comparisons of mineralogy with age, latitude, and elevation, only pixels with summed concentrations greater than 0.5 for each group are used. A generalized age map (Figure 7) was compiled using the simple cylindrical global geologic unit maps of *Scott and Tanaka* [1986], *Greeley and Guest* [1987], and *Tanaka and Scott* [1987]. Transitional units between Noachian and Hesperian and between Hesperian and Amazonian ages were grouped into the younger of the two ages, after *Solomon et al.* [2005]. A MOLA elevation map was generated from the MGS Mars Orbiter Laser Altimeter (MOLA) elevation data binned at 128 pixels-per-degree [*Smith et al.*, 2001].

[27] Surfaces with the highest abundance of high-silica phase(s) (Group 1) are concentrated in the northern lowlands, Solis Planum, and scattered throughout the southern mid- to high-latitude regions. Surfaces with the lowest abundance of high-silica phase(s) (Groups 2–4) are concentrated throughout the southern highlands, including southern mid- to high-latitude regions. Nearly all of the occurrences (~85%) of the N. Acidalia-Solis Planum group (Group 1) with concentrations greater than 0.5 are located in Hesperian terrains (Figure 7). With the exception of surfaces in Solis Planum, Group 1 is primarily found at latitudes greater than ~45°N, with a few occurrences found south of 45°S (Figure 8), generally between ~90°E and 270°E. Whereas the northern high latitudes are dominated by

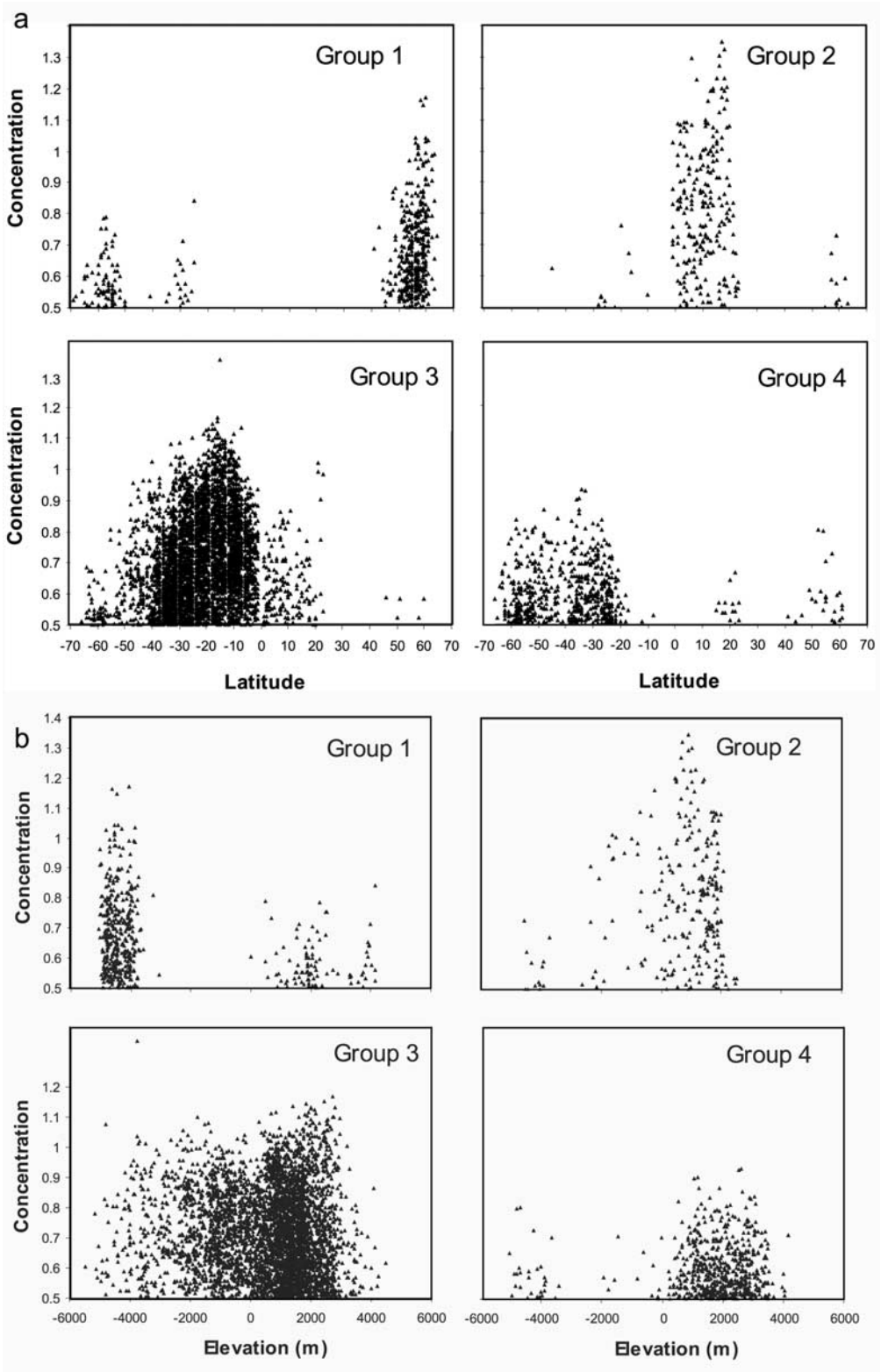

Figure 8. Summed spectral concentrations for the composition groups shown in Figure 7 plotted as a function of (a) latitude and (b) altitude. The northern Acidalia + Solis Planum group is primarily found at latitudes >45°. The remaining groups are mainly located southward of 20°N, in the cratered highlands.

Group 1, the southern high latitudes contain additional groups. Finally, although there are several Group 1 surfaces located at elevations between 500 and 4000 m above datum, most of the elevated concentrations are found at low altitudes (Figure 8).

[28] Group 2 is located almost exclusively in Syrtis Major. Approximately 95% of the Group 2 occurrences with >0.5 concentration are found associated with Hesperian-aged surfaces.

[29] Group 3 is located exclusively in the southern highlands, and is the most widespread of the four units. Approximately 75% of the Group 3 surfaces with >0.5 concentration are found in Noachian terrains, whereas 25% are found in Hesperian terrains (Figure 7). Elevated concentrations are generally only found south of 20°N, but they are found over a wide range of altitudes (Figure 8).

[30] Group 4 is located primarily in the southern highlands, south of 20°S latitude, with approximately 45% of Group 4 occurrences in Noachian terrains and 55% found in Hesperian terrains. The majority of Group 4 occurrences are found in low-albedo areas surrounding the Tharsis province (Figure 7). Group 4 concentrations greater than 0.5 are generally found at elevations between 500 and 4000 m above datum (Figure 8).

4.4. Comparison With Previous Spectroscopic Results

[31] In general, the derived modal mineralogy for each representative shape compares well with the mineral concentration maps of *Bandfield* [2002, 2003], once normalized for blackbody. Regions modeled with the highest abundance of high-silica phase(s) are northern Acidalia and Solis Planum, in agreement with *Bandfield et al.* [2000] and *Bandfield* [2002, 2003]. Regions modeled with the highest abundance of clinopyroxene are Syrtis Major, Tyrrhena Terra, Cimmeria Terra, Iapygia, Protei Regio, Sinus Meridiani and areas in Sinus Margaritifer [*Bandfield*, 2002], also in agreement with this study. In this work, plagioclase abundance is relatively constant on a global scale (varying between ~25 and 35%), with Hesperia, Tyrrhena and Meridiani having the lowest abundances. Normalized plagioclase abundance maps from *Bandfield* [2002, 2003] also show a narrow range of abundances between 25 and 35%, with Meridiani and Hesperia having some of the lowest abundances; however in that work, areas in Thaumasia, Mare Sirenum and parts of Cimmeria also have slightly lower plagioclase abundances. Finally, areas with the highest plagioclase to pyroxene ratios of *Bandfield* [2002, 2003] are Acidalia, western Solis Planum, Pandorae Fretum, and the southern mid- to high-latitude regions, similar to this work (Table 2).

[32] Notable differences between this work and that of *Bandfield* [2002] are that Solis Planum is modeled with ~10% lower high-silica phase(s) abundance and ~10% greater orthopyroxene abundance in this study. In addition, some parts of the northern Acidalia region are modeled with a lower total pyroxene abundance in the work of *Bandfield* [2002] compared to this study. Finally, Aonium Sinus has the highest plagioclase to pyroxene ratio in this study; however, this region does not stand out in a plagioclase/pyroxene ratio map derived from the distributions of *Bandfield* [2002, 2003]. Inconsistencies between the results of this and previous work are due to the following: (1) differences in wavelength range used for spectral fitting, (2) differences in spectral libraries used for modeling (particularly the addition of olivine spectra [*Hamilton and Schneider*, 2005]), (3) the use of multiple libraries versus a single library to derive modal mineralogy, and (4) differences in the approach to mapping spatial variations in mineralogy (section 3).

[33] The distributions of relative differences in mafic mineral abundances from this work are generally consistent with VIS/NIR observations from ISM [*Mustard et al.*, 1993; *Mustard and Sunshine*, 1995; *Mustard et al.*, 1997] and Mars Express OMEGA [*Bibring et al.*, 2005; *Mustard et al.*, 2005; *Le Mouélic et al.*, 2006]. Because some regions are modeled as mixtures of more than one spectral class, direct correlation of unit distributions with OMEGA maps are precluded. However, the major similarities are presented here. Martian dark regions in the southern highlands are dominated by high-Ca clinopyroxene-bearing basaltic rocks, similar to VIS/NIR results [*Mustard et al.*, 1993; *Bibring et al.*, 2005; *Mustard et al.*, 2005]. In the southern highlands regions, orthopyroxenes are modeled at lower concentrations than high-Ca clinopyroxenes, also consistent with VIS/NIR observations [*Bibring et al.*, 2005; *Mustard et al.*, 2005]. Southern highlands areas with greatest low-Ca pyroxene abundance mapped thus far by OMEGA include Cimmeria, Iapygia, and parts of Meridiani and Margaritifer Sinus, which is mostly consistent with this work (the low-Ca pyroxene abundance modeled for Meridiani in this work is lower than that of Cimmeria-Iapygia, section 4.2). A particularly good correlation between the data sets is found near the southern boundary of Syrtis Major, where there is a notable difference in low-Ca pyroxene abundance between Syrtis and Iapygia in OMEGA mineral maps [*Bibring et al.*, 2005]. This difference is also observed in TES data (Figures 5 and 7). Gaps in OMEGA coverage preclude comparison for all regions with relatively higher low-Ca pyroxene abundances (e.g., Solis Planum) from this study. As additional OMEGA data are obtained, further comparisons to the results of this study can be made.

[34] Although both TES and OMEGA results indicate that the northern plains exhibit the lowest total abundance of pyroxene of all low-albedo regions, one apparent discrepancy between the two data sets is that low-Ca pyroxene is modeled at higher abundance than high-Ca pyroxene in northern Acidalia with TES data (Table 2) [see also *Bandfield*, 2002, Figure 2]. Conversely, the OMEGA team reports that only high-Ca pyroxene is present in the northern plains, and at low abundance [*Bibring et al.*, 2005; *Mustard et al.*, 2005]. Exclusion of low-Ca pyroxenes from the end-member set does to some extent adversely affect the model fit to the northern Acidalia spectral shape (RMS error of 0.136% versus 0.187%), suggesting that they are important components. Although *Bibring et al.* [2005] report that only high-Ca pyroxene is present in the northern lowlands, OMEGA pyroxene abundance maps do show that parts of northern Acidalia and northern Utopia exhibit higher abundance of low-Ca pyroxene than high-Ca pyroxene [*Bibring et al.*, 2005]. These are the areas from where TES spectra were extracted to produce the northern Acidalia representative shape (Paper 1). Additionally, preliminary mineral maps produced by *Le Mouélic et al.* [2006] with OMEGA data also suggest the presence of orthopyroxene in northern

Acidalia, so it may be that the two data sets are in agreement in these areas.

5. Discussion

5.1. Global Compositional Trends

[35] On the basis of differences in plagioclase, pyroxene, olivine, and high-silica phase abundance, the nine representative spectral shapes from low-albedo regions (Figure 2) were divided into four groups (section 4.2). The spectral differences between these four groups are subtle; however they are comparable to spectral variation associated with terrestrial mafic and intermediate volcanic rocks (Figure 6). Given the regional averaging used to produce the representative spectra (Paper 1), and the previous evidence that Mars has probably experienced little crustal recycling [e.g., *Borg et al.*, 1997; *Zuber*, 2001; *McSween et al.*, 2003; *Wieczorek and Zuber*, 2004] and limited chemical weathering [e.g., *Christensen et al.*, 2001; *Goetz et al.*, 2005; *Haskin et al.*, 2005; *Yen et al.*, 2005; *Christensen et al.*, 2005; *Hamilton et al.*, 2005], the lack of extreme spectral variations measured in this work (that might be expected for concentrated secondary mineralization or silicic crust) is not surprising.

[36] By classifying the representative spectral shapes into four groups, distinct boundaries are, by definition, imposed on these spectral classes. In actuality, the mineralogic differences are more gradational within and between each group (Table 2). In particular, Group 3 exhibits the most variability in derived mineralogy. Although it is primarily distinguished by relatively low plagioclase, intermediate high-Ca pyroxene, and high olivine abundance, the abundance of low-Ca pyroxene varies by ~10%. Nonetheless, these divisions help to visualize global-scale spatial trends in modal mineralogy.

[37] The minimum mineral abundance differences that separate Groups 2–4 are ~10–15%, which is the traditional detection limit for TES data [*Christensen et al.*, 2000a]. In addition, in this work we report and interpret ~10% differences in olivine and low-Ca pyroxene abundance as part of overall unit composition, even though these phases are modeled at or close to the detection limit. The variations in low-Ca pyroxene abundance reported here are largely in agreement with those observed in OMEGA data. For the following discussion, we accept the global-scale compositional trends apparent from this study as accurate and interpret them. Future work that re-addresses detection limits defined for TES data may help to validate the mineralogic divisions suggested here. Regardless of the mineralogic interpretations, it is important to note that the spectral differences between these regions are valid (Paper 1); mineralogic estimates may be refined in the future as more information becomes available.

5.2. Implications for Surface Alteration

[38] On the ternary plot of plagioclase – ferromagnesian silicates – high-silica phase(s), there is no single trend toward increasing abundance of high-silica phase(s) or toward any particular mineral group (Figure 5a). Thus these global trends cannot be attributed entirely to weathering of feldspars and/or mafic minerals and subsequent formation of phyllosilicates or allophane/amorphous silica. Compositional units between 45°S and 45°N (Groups 2–4) exhibit moderate correlation with distinct terrains defined by large-scale morphology, geographic/topographic province, and to some extent, surface age, suggesting control by primary bedrock units (Figure 7). For example, although high-silica phase(s) also differ, the most significant differences between Groups 2 and 3 are that Group 3 has a ~10% lower high-Ca pyroxene abundance and ~10% higher abundance of low-Ca pyroxene. These mineralogic changes are also observed in OMEGA data, especially for Syrtis Major and surrounding areas. For Groups 3 and 4, high-silica phase abundances are similar, and compositional differences are primarily with plagioclase, low-Ca pyroxene and olivine abundance. It is difficult to imagine a weathering scenario that could produce the observed relative differences in high- and low-Ca pyroxene. In summary, these observations indicate that alteration is not a significant process contributing to spectral variations in low-albedo regions equatorward of ±45° latitude. Differences in the primary mineralogy of crust-forming lavas dominate the spectral variations observed with TES data.

[39] The Northern Acidalia + Solis spectral group (Group 1), which is dominated by high-silica phase(s) (>30%), and generally corresponds to the original Surface Type 2 spectral shape derived by *Bandfield et al.* [2000], is found primarily at latitudes greater than 45° (Figure 8a). This distribution strongly suggests that high-latitude (>45°) occurrences of high-silica phase(s) are alteration products (amorphous to poorly crystalline aluminosilicates or zeolites, section 2.1.). As previously suggested by *Wyatt et al.* [2004] and *Michalski et al.* [2005a], surface alteration at high latitudes was likely enabled by the availability of surface H_2O and possibly linked to the locations of once-present snow deposits [*Mustard et al.*, 2001; *Christensen*, 2003; *Milliken et al.*, 2003].

[40] The possibility that high-latitude occurrences of high-silica phase(s) are due to alteration raises additional questions about when the alteration occurred and what the composition of the unaltered substrate was. It is unclear how long coatings could survive on sand grains in an active, saltating environment (see Paper 1 for a lengthier discussion), but it is likely that coatings would eventually be removed after a large (though unknown) number of saltation impacts [e.g., *Sagan*, 1973; *Huguenin*, 1976; *Greeley et al.*, 1982; *Kraft and Greeley*, 2000]. This suggests that high-latitude surface alteration occurred either relatively recently, or that altered sands were recently exposed. Alternatively, it is possible that the rate of coating formation exceeds or equals that of coating removal, and coatings may have been formed and removed repeatedly throughout Mars' history.

[41] The composition of the unaltered or uncoated substrate from which Group 1 may have been derived is also of interest. Was it similar to or different than the average highlands composition? First, the pyroxene mineralogy of the plains of northern Acidalia and other high-silica surfaces are dominated by the low-Ca variety (Table 2). This mineralogy is unlike the highlands, where high-Ca pyroxene is the dominant pyroxene (Table 2). In addition, high-latitude, high-silica surfaces (Group 1) exhibit more than 10% lower pyroxene abundance, and ~5% greater plagioclase abundance relative to the average and most widespread basalt composition in the equatorial and midlatitude regions (Group 3). Thus if the Group 1 surfaces consist

simply of average highlands basalt that was altered to produce high-silica coatings, the implication is that pyroxene was strongly preferentially weathered to produce high-silica phase(s). Experimental weathering studies suggest that either plagioclase or pyroxene can be preferentially dissolved from basalts, depending on the solution conditions (e.g., pH, temperature) [e.g., *Hurowitz et al.*, 2005; *McAdam et al.*, 2006]. If preferential weathering of an average highlands basalt did occur, then uniform weathering conditions across Group 1 areas are implied. This is not an unreasonable suggestion, however, given the difference in pyroxene mineralogy described above, we think a more likely explanation is that the substrate lithology was different than that of the average highlands (Group 3). That substrate mineralogy might have consisted of a higher plagioclase abundance, and possibly higher abundance of less-stable phases such as glass and/or olivine [e.g., *Colman*, 1982; *Tosca et al.*, 2004] relative to pyroxene, compared to the average highlands composition. The substrate lithology for surfaces dominated by high-silica phase(s) is not required to be the same at both northern and southern high latitudes. For example, the northern plains of Acidalia may have contained a higher fraction of olivine or glass, whereas the southern high latitudes may have contained a higher fraction of plagioclase. In summary, we suggest that differences between Group 1 surfaces and the average highlands basalt (Group 3) could be due to a combination of igneous and alteration processes.

[42] It is important to note that units equatorward of 45° contain 10–20% abundance of high-silica phase(s). In addition, there are three regions that are dominated by high-silica phase(s) (>30%), in which a primary origin for the high-silica phase(s) is either more likely or just as likely as a secondary origin. These are Solis Planum (latitude $\cong$ 28°S), the north polar dunes [*Bandfield et al.*, 2002], and lava flows in Nili Patera [*Christensen et al.*, 2005]. A primary origin is particularly evident in the Nili Patera region, where the geologic context strongly argues for the presence of volcanic glass [*Christensen et al.*, 2005]. Nili Patera contains a well-defined $\sim$1090 cm^{-1} feature that is clearly better fit with obsidian glass than phyllosilicates [*Christensen et al.*, 2005], indicating that secondary high-silica phases in the form of phyllosilicates may be ruled out. However, zeolites and secondary amorphous silica probably cannot be discounted on that basis. The stubby lava flow that contains $\sim$30% high-silica phases overlies a basaltic caldera floor, in which only $\sim$5% high-silica phases are modeled [*Christensen et al.*, 2005, Figures 4 and 5]. Both units contain $\sim$35% plagioclase. It seems unlikely that the younger unit would contain a greater abundance of alteration phases, whereas the older basaltic unit would have essentially none. Thus the stratigraphic relationship of these units suggests that the high-silica phase is primary in origin. Finally, ''Clovis''-class rocks in the Columbia Hills of Gusev Crater appear to be dominated by basaltic glass-like components [*Ruff and the Athena Science Team*, 2006], despite the fact that these rocks may have undergone substantial alteration [*Squyres et al.*, 2006]. The Columbia Hills and Nili Patera are at least Hesperian in age, which suggests that glasses have been capable of surviving billions of years on the Martian surface without having been completely weathered away. Therefore it is not unreasonable to suggest that glasses may indeed be contributing to the high-silica phase(s) detected by TES in other areas. Either way, the global occurrences of surfaces dominated by high-silica phases (e.g., high latitudes, Solis Planum, Nili Patera) indicate that more than one process produced large areas dominated by these phases on Mars. Both volcanic and alteration mechanisms remain viable explanations for all high-silica surfaces on Mars.

5.3. Implications for Crustal Development

[43] Results from this work confirm those of previous studies [*Bandfield et al.*, 2000; *Christensen et al.*, 2000a; *Bandfield*, 2002; *Hamilton et al.*, 2003a; *McSween et al.*, 2003], that there is a substantial fraction of plagioclase (>$\sim$25%) present in Martian low-albedo regions, including Noachian and Hesperian terrains. It has been suggested that Noachian-aged lithologies that contain both low- and high-Ca pyroxenes were derived from source regions that were strongly depleted in aluminum [*Mustard et al.*, 1997, 2005]. However, these outcrops are located in terrains that contain abundant plagioclase. Thus those source regions could not have already been strongly Al-depleted; however, perhaps the formation of those ancient terrains contributed to the Al-depletion event, as previously suggested by *Hamilton et al.* [2003a].

[44] It is possible that the high modal abundances of plagioclase were achieved through fractional crystallization of melts from Al-depleted sources; however, there is specific confirmation of the existence of at least one early Hesperian-aged Al-undepleted source region [*McSween et al.*, 2006]. APXS measurements of fresh surfaces of Gusev plains basalts revealed Mg/Al and Al/Si ratios similar to terrestrial basalts, and >35% normative plagioclase [*Gellert et al.*, 2004; *Christensen et al.*, 2004; *McSween et al.*, 2004, 2006]. The basalts contain up to 30% olivine, which is probably phenocrystic, suggesting that Gusev magmas (and presumably their Al-contents) were not affected by significant fractionation [*McSween et al.*, 2006]. Despite the low abundances of incompatible elements and presence of normative hypersthene plus olivine in Gusev basalts [*McSween et al.*, 2004], *McSween et al.* [2006] conclude that Al-undepleted mantle sources must have persisted after the Noachian time period.

[45] Whereas the Noachian terrains do not show evidence of source regions that were already strongly Al-depleted, plagioclase/pyroxene ratios do vary within the southern highlands (Table 2), which span a range of ages. From this study it should be possible to investigate whether progressive Al removal from the mantle is recorded between Noachian and Hesperian terrains. In a simple model of continued melt extraction from mantle reservoirs that produced Noachian crust, unmodified, primitive melts that formed Hesperian lavas should contain less Al than the older crust. Accordingly, modal proportions of plagioclase should decrease from Noachian to Hesperian terrains. However, a decrease in plagioclase abundance is not observed between Noachian and Hesperian surfaces (e.g., between Groups 3 and 2, or Groups 3 and 4, or, within Group 3). This indicates that additional processes must have affected Hesperian mantle melts (loosely represented by Groups 2 and 4). One explanation is that lavas in Group 2 terrains may have undergone increased fractionation of low-Ca

pyroxene and olivine, relative to Group 3 terrains. Alternatively, these magmas may have had a significant assimilated crustal component. Finally, it is also possible that Syrtis and other Hesperian lavas may have been derived by partial melting of another source (the crust). Because the degree of fractionation and/or assimilation is unknown, it is difficult to constrain the Al-depletion state of the Group 2 and 4 (generally, Hesperian-aged) source regions. It is not clear if the original, unmodified melts were derived from a relatively undepleted mantle source, such as that of Gusev crater basalts, or a slightly Al-depleted source relative to Noachian magma source regions.

[46] Another example of possible melt modification by fractionation is the Aonium-Phrixi compositional unit (Group 4). Group 4 surfaces exhibit a decreased abundance of olivine, and increased plagioclase/pyroxene ratio, relative to Group 3. The most spatially contiguous concentration of Group 4 surfaces is broadly correlated with Hesperian units near the Tharsis plateau. In this example, it is possible that olivine and pyroxene were preferentially weathered from Group 4. However, Group 4 surfaces are located in topographically high areas relative to Group 3 (Figure 8b), suggesting that alteration is a less probable explanation for the observed differences because liquid water is less likely to be stable. An alternative explanation for the relative decrease in olivine abundance is that magmas in Group 4 regions underwent a slightly higher degree of olivine fractionation. If the observed topographic high in the Thaumasia/Aonium/Phrixi area is due to isostatic adjustment of a relatively uniform-density crust (e.g., the Group 4 composition is not representative of rock composition at depth in this region), then the crust may be thicker in this area [e.g., *Zuber et al.*, 2000]. The thicker crust could have facilitated the increased fractionation of olivine relative to other highland terrains. Alternatively, if this compositional unit does extend at depth, compensation of the associated topographic high in Thaumasia/Aonium/Phrixi may have been achieved by a decrease in crustal density in this region.

[47] In the preceding paragraphs we have mostly discussed the implications for the type localities of the spectral classes derived in this work. The explanations given may not apply to all of these regions. For example, the Pandorae region, which is dominated by the Aonium-Phrixi spectral class (Group 4), may have a different explanation for the observed mineralogy. Similarly, Hesperia Planum probably has a different history than Sinus Meridiani, even though they are both in Group 3. In summary, we have addressed some geological implications of the global-scale trends, but regional-scale differences in geologic history are almost certain.

6. Conclusions

[48] Mars is a planet with a complex history influenced by volcanic, hydrologic and sedimentary process; therefore a simple model of crustal evolution and surface alteration should not be expected. It is likely that all of these processes have contributed to the global compositional trends identified in this work. Only detailed studies using multiple wavelength regions and geologic context, improved spatial resolution, and future rover missions will help to gradually unravel the complex geologic history of Mars. Neither a primary nor a secondary origin for the high-silica component measured with TES can be ruled out; and, this work does not unequivocally determine that observed variations in mineralogy are caused only by original crustal variations in primary mineralogy or solely by weathering processes. Nevertheless, the following conclusions may be made.

[49] 1. Martian low-albedo regions primarily consist of plagioclase, pyroxene, olivine, and high-silica phase(s). Low-albedo regions were classified into four groups, based on relative abundances of these phases.

[50] 2. Mineralogic variations associated with original crust-forming magmas are at least partially responsible for the observed spectral differences between some Martian low-albedo regions.

[51] 3. Some Hesperian terrains exhibit a difference in mineralogy from Noachian terrains and from each other, suggesting variations in the degree of crystal fractionation, assimilation, and/or source region compositions. Areas in topographically high regions near the Tharsis Plateau (e.g., Thaumasia, Aonium Sinus, Phrixi Regio) exhibit lower abundances of olivine and greater plagioclase/pyroxene ratios than surrounding highland terrains, suggesting that magmas in this region may have undergone increased olivine fractionation, possibly facilitated by thicker crust.

[52] 4. Surfaces with the greatest abundance of high-silica phase(s) are primarily found in latitudes poleward of $\pm 45°$. Elevated abundances are also located in western Solis Planum (this work and *Bandfield* [2002]). High-latitude high-silica phase(s) are probably secondary in nature, as suggested by previous authors [*Wyatt et al.*, 2004; *Michalski et al.*, 2005a]; however, a volcanic origin cannot be ruled out. In other regions, such as in Nili Patera, high-silica phase(s) are probably primary in origin [*Christensen et al.*, 2005] (also this paper, section 5.2). It is likely that both magmatic and alteration processes are contributing to the observed global distribution of high-silica phase(s).

[53] 5. If the high-latitude high-silica phases are secondary, the substrate mineralogy was likely different than that of the average cratered highlands. That original mineralogy for the high-silica surfaces is not required to be the same for both the northern and southern high-latitude regions. Thus both igneous and alteration processes may be contributing to the spectral differences between Group 1 and Group 3 surfaces. These groups loosely correspond to the original Surface Type 2 and Surface Type 1 terrains defined by *Bandfield et al.* [2000].

[54] 6. Results from this work are consistent with most of the major results from previous orbital spectroscopic analyses, in that (1) plagioclase and high-Ca clinopyroxene are the dominant components of most southern highlands regions, (2) the highest concentrations of high-silica phase(s) are found in the northern plains, Solis Planum and a few southern high-latitude regions, and (3) the northern plains exhibit the lowest pyroxene abundance within Mars' low-albedo regions.

[55] **Acknowledgments.** We are grateful to Josh Bandfield, who contributed significantly to the discussion presented in this paper, and prompted our thinking and development of ideas about the substrate mineralogy of high-silica surfaces. We thank Mike Kraft and Tim Glotch for constructive reviews of early versions of this manuscript, and Vicky Hamilton for graciously providing the olivine solid solution and pigeonite spectra. We sincerely appreciate Oded Aharonson's assistance with the

constrained nonnegative least squares fitting routines and for suggesting their use in this work. John Holloway, Hap McSween, Tom Sharp, Matt Fouch, Steve Ruff and Mike Wyatt provided valuable discussions of our results. Formal and thorough reviews from Michelle Minitti and Michael Ramsey significantly improved this manuscript, and are much appreciated. The Mars Global Surveyor Project Office provided support for this work.

References

Aben, L. K. (2003), Compositional and thermophysical analysis of Martian aeolian dunes, M. S. thesis, 117 pp., Ariz. State Univ., Tempe.

Adams, J. B., and T. B. McCord (1969), Mars: Interpretation of spectral reflectivity of light and dark regions, *J. Geophys. Res.*, *74*(20), 4851–4856.

Aharonson, O., M. T. Zuber, D. H. Rothman, N. Schorghofer, and K. X. Whipple (2002), Drainage basins and channel incision on Mars, *Proc. Natl. Acad. Sci. U. S. A.*, *99*(4), 1780–1783.

Anderberg, M. R. (1973), *Cluster Analysis for Applications*, 359 pp., Elsevier, New York.

Arvidson, R. E., F. Poulet, J. P. Bibring, M. Wolff, A. Gendrin, R. V. Morris, J. J. Freeman, Y. Langevin, N. Mangold, and G. Bellucci (2005), Spectral reflectance and morphologic correlations in Eastern Terra Meridiani, Mars, *Science*, *307*, 1591–1594.

Bandfield, J. L. (2002), Global mineral distributions on Mars, *J. Geophys. Res.*, *107*(E6), 5043, doi:10.1029/2001JE001802.

Bandfield, J. L. (2003), Martian global surface mineralogy from the Thermal Emission Spectrometer: Surface emissivity, mineral map, and spectral end-member data products, paper presented at Sixth International Conference on Mars, Calif. Inst. of Technol., Pasadena.

Bandfield, J. L., and M. D. Smith (2003), Multiple emission angle surface-atmosphere separations of Thermal Emission Spectrometer data, *Icarus*, *161*(1), 47–65.

Bandfield, J. L., V. E. Hamilton, and P. R. Christensen (2000), A global view of Martian surface compositions from MGS-TES, *Science*, *287*, 1626–1630.

Bandfield, J. L., K. S. Edgett, and P. R. Christensen (2002), Spectroscopic study of the Moses Lake dune field, Washington: Determination of compositional distributions and source lithologies, *J. Geophys. Res.*, *107*(E11), 5092, doi:10.1029/2000JE001469.

Bandfield, J. L., V. E. Hamilton, P. R. Christensen, and H. Y. McSween Jr. (2004), Identification of quartzofeldspathic materials on Mars, *J. Geophys. Res.*, *109*, E10009, doi:10.1029/2004JE002290.

Barrat, J. A., A. Jambon, M. Bohn, P. Gillet, V. Sautter, C. Gopel, M. Lesourd, and F. Keller (2002), Petrology and chemistry of the picritic shergottite North West Africa 1068 (NWA 1068), *Geochim. Cosmochim. Acta*, *66*(19), 3505–3518.

Bell, J. F., M. J. Wolff, P. B. James, R. T. Clancy, S. W. Lee, and L. J. Martin (1997), Mars surface mineralogy from Hubble Space Telescope imaging during 1994–1995: Observations, calibration, and initial results, *J. Geophys. Res.*, *102*(E4), 9109–9123.

Bibring, J. P., et al. (1990), Ism observations of Mars and Phobos—1st results, *Proc. Lunar Planet. Sci. Conf.*, *20*, 461–471.

Bibring, J. P., et al. (2005), Mars surface diversity as revealed by the OMEGA/Mars Express observations, *Science*, *307*, 1576–1581.

Blaney, D. L., D. A. Glenar, and G. L. Bjorker (2003), High spectral resolution spectroscopy of Mars from 2 to 4 microns: Surface mineralogy and the atmosphere, paper presented at Sixth International Conference on Mars, Calif. Inst. of Technol., Pasadena.

Borg, L. E., L. E. Nyquist, L. A. Taylor, H. Wiesmann, and C. Y. Shih (1997), Constraints on Martian differentiation processes from Rb-Sr and Sm-Nd isotopic analyses of the basaltic shergottite QUE 94201, *Geochim. Cosmochim. Acta*, *61*(22), 4915–4931.

Carr, M. H. (1996), *Water on Mars*, Oxford Univ. Press, New York.

Christensen, P. R. (2003), Formation of recent Martian gullies through melting of extensive water-rich snow deposits, *Nature*, *422*(6927), 45–48.

Christensen, P. R., and S. W. Ruff (2004), The formation of the hematite-bearing unit in Meridiani Planum: Evidence for deposition in standing water, *J. Geophys. Res.*, *109*, E08003, doi:10.1029/2003JE002233.

Christensen, P. R., J. L. Bandfield, M. D. Smith, V. E. Hamilton, and R. N. Clark (2000a), Identification of a basaltic component on the Martian surface from Thermal Emission Spectrometer data, *J. Geophys. Res.*, *105*(E4), 9609–9621.

Christensen, P. R., et al. (2000b), Detection of crystalline hematite mineralization on Mars by the Thermal Emission Spectrometer: Evidence for near-surface water, *J. Geophys. Res.*, *105*(E4), 9623–9642.

Christensen, P. R., J. L. Bandfield, V. E. Hamilton, D. A. Howard, M. D. Lane, J. L. Piatek, S. W. Ruff, and W. L. Stefanov (2000c), A thermal emission spectral library of rock-forming minerals, *J. Geophys. Res.*, *105*(E4), 9735–9739.

Christensen, P. R., et al. (2001), Mars Global Surveyor Thermal Emission Spectrometer experiment: Investigation description and surface science results, *J. Geophys. Res.*, *106*(E10), 23,823–23,871.

Christensen, P. R., et al. (2003), Morphology and composition of the surface of Mars: Mars Odyssey THEMIS results, *Science*, *300*, 2056–2061.

Christensen, P. R., et al. (2004), Initial results from the Mini-TES experiment in Gusev crater from the Spirit rover, *Science*, *305*, 837–842.

Christensen, P. R., et al. (2005), Evidence for magmatic evolution and diversity on Mars from infrared observations, *Nature*, *436*, 504–509.

Colman, S. M. (1982), Chemical weathering of basalts and andesites: Evidence from weathering rinds, report, 51 pp., Geol. Surv., U. S. Dep. of the Interior, Washington, D. C.

Edgett, K. S., and P. R. Christensen (1991), The particle-size of Martian aeolian dunes, *J. Geophys. Res.*, *96*(E5), 22,765–22,776.

Eggleton, R. A., C. Foudoulis, and D. Varkevisser (1987), Weathering of basalt—Changes in rock chemistry and mineralogy, *Clays Clay Miner.*, *35*(3), 161–169.

Erard, S., J. P. Bibring, J. Mustard, O. Forni, J. W. Head, S. Hurtrez, Y. Langevin, C. M. Pieters, J. Rosenqvist, and C. Sotin (1991), Spatial variations in composition of the Valles Marineris and Isidis Planitia regions of Mars derived from Ism data, *Proc. Lunar Planet. Sci.*, *21*, 437–455.

Feely, K. C., and P. R. Christensen (1999), Quantitative compositional analysis using thermal emission spectroscopy: Application to igneous and metamorphic rocks, *J. Geophys. Res.*, *104*(E10), 24,195–24,210.

Gellert, R., et al. (2004), Chemistry of rocks and soils in Gusev crater from the alpha particle x-ray spectrometer, *Science*, *305*, 829–832.

Gendrin, A., et al. (2005), Sulfates in Martian layered terrains: The OMEGA/Mars Express view, *Science*, *307*, 1587–1591.

Glotch, T. D., and J. L. Bandfield (2006), Determination and interpretation of surface and atmospheric Mini-TES spectral end-members at the Meridiani Planum landing site, *J. Geophys. Res.*, *111*, E12S06, doi:10.1029/2005JE002671.

Glotch, T. D., and P. R. Christensen (2005), Geologic and mineralogic mapping of Aram Chaos: Evidence for a water-rich history, *J. Geophys. Res.*, *110*, E09006, doi:10.1029/2004JE002389.

Glotch, T. D., R. V. Morris, P. R. Christensen, and T. G. Sharp (2004), Effect of precursor mineralogy on the thermal infrared emission spectra of hematite: Application to Martian hematite mineralization, *J. Geophys. Res.*, *109*, E07003, doi:10.1029/2003JE002224.

Glotch, T. D., D. Rogers, and P. R. Christensen (2005), A newly discovered hematite-rich unit in Aureum Chaos: Comparison of hematite and associated units with those in Aram Chaos, *Lunar Planet. Sci.*, [CD-ROM], *XXXVI*, abstract 2159.

Goetz, W., et al. (2005), Indication of drier periods on Mars from the chemistry and mineralogy of atmospheric dust, *Nature*, *436*(7047), 62–65.

Goodrich, C. A. (2003), Petrogenesis of olivine-phyric shergottites Sayh Al Uhaymir 005 and elephant moraine A79001 lithology A, *Geochim. Cosmochim. Acta*, *67*(19), 3735–3772.

Greeley, R., and J. E. Guest (1987), Geologic map of the eastern equatorial region of Mars, *U.S. Geol. Surv. Misc. Invest. Ser. Map*, I-1802-B.

Greeley, R., and M. D. Kraft (2001), Survivability of aggregate sands on Mars, *Lunar Planet. Sci.*, *XXXII*, abstract 1839.

Greeley, R., R. N. Leach, S. H. Williams, B. R. White, J. B. Pollack, D. H. Krinsley, and J. R. Marshall (1982), Rate of wind abrasion on Mars, *J. Geophys. Res.*, *87*(B12), 9–24.

Grieve, R. A. F., F. Langenhorst, and D. Stoffler (1996), Shock metamorphism of quartz in nature and experiment: 2. Significance in geoscience, *Meteorit. Planet. Sci.*, *31*(1), 6–35.

Hale, V. P. S., H. Y. McSween, and G. A. McKay (1999), Re-evaluation of intercumulus liquid composition and oxidation state for the Shergotty meteorite, *Geochim. Cosmochim. Acta*, *63*(9), 1459–1470.

Hamilton, V. E. (2000), Thermal infrared spectroscopy of the pyroxene mineral series, *J. Geophys. Res.*, *105*(E4), 9701–9716.

Hamilton, V. E. (2004), Detailed investigation of a globally unique, orthopyroxene-rich deposit of Eos Chasma, *Mars, Eos. Trans. AGU*, *85*(47), Fall Meet. Suppl., Abstract P11A-0959.

Hamilton, V. E. (2005), Small, spectrally distinct deposits in the Valles Marineris, Mars: A new lithology?, *Eos. Trans. AGU*, *86*(52), *Fall Meet. Suppl.*, Abstract P24A-08.

Hamilton, V. E., and P. R. Christensen (2000), Determining the modal mineralogy of mafic and ultramafic igneous rocks using thermal emission spectroscopy, *J. Geophys. Res.*, *105*(E4), 9717–9733.

Hamilton, V. E., and P. R. Christensen (2005), Evidence for extensive, olivine-rich bedrock on Mars, *Geology*, *33*(6), 433–436.

Hamilton, V. E., and R. D. Schneider (2005), Alteration phases associated with high concentrations of orthopyroxene and olivine on Mars, *Lunar Planet. Sci.*, *XXXVI*, abstract 2212.

Hamilton, V. E., M. B. Wyatt, H. Y. McSween, and P. R. Christensen (2001), Analysis of terrestrial and Martian volcanic compositions using thermal emission spectroscopy: 2. Application to Martian surface spectra from the Mars Global Surveyor Thermal Emission Spectrometer, *J. Geophys. Res.*, *106*(E7), 14,733–14,746.

Hamilton, V. E., P. R. Christensen, H. Y. McSween, and J. L. Bandfield (2003a), Searching for the source regions of Martian meteorites using MGS TES: Integrating Martian meteorites into the global distribution of igneous materials on Mars, *Meteorit. Planet. Sci.*, *38*(6), 871–885.

Hamilton, V. E., P. R. Christensen, and J. L. Bandfield (2003b), Volcanism or aqueous alteration on Mars?, *Nature*, *421*(6924), 711–712.

Hamilton, V. E., H. Y. McSween Jr., and B. Hapke (2005), Mineralogy of Martian atmospheric dust inferred from thermal infrared spectra of aerosols, *J. Geophys. Res.*, *110*, E12006, doi:10.1029/2005JE002501.

Haskin, L. A., et al. (2005), Water alteration of rocks and soils on Mars at the Spirit rover site in Gusev crater, *Nature*, *436*(7047), 66–69.

Hoefen, T. M., R. N. Clark, J. L. Bandfield, M. D. Smith, J. C. Pearl, and P. R. Christensen (2003), Discovery of olivine in the Nili Fossae region of Mars, *Science*, *302*, 627–630.

Howard, A. D., J. M. Moore, and R. P. Irwin III (2005), An intense terminal epoch of widespread fluvial activity on early Mars: 1. Valley network incision and associated deposits, *J. Geophys. Res.*, *110*, E12S14, doi:10.1029/2005JE002459.

Huguenin, R. L. (1976), Mars—Chemical weathering as a massive volatile sink, *Icarus*, *28*(2), 203–212.

Hurowitz, J. A., S. McLennan, D. H. Lindsley, and M. A. A. Schoonen (2005), Experimental epithermal alteration of synthetic Los Angeles meteorite: Implications for the origin of Martian soils and identification of hydrothermal sites on Mars, *J. Geophys. Res.*, *110*, E07002, doi:10.1029/2004JE002391.

Hynek, B. M., and R. J. Phillips (2003), New data reveal mature, integrated drainage systems on Mars indicative of past precipitation, *Geology*, *31*(9), 757–760.

Irwin, R. P., III, A. D. Howard, R. A. Craddock, and J. M. Moore (2005), An intense terminal epoch of widespread fluvial activity on early Mars: 2. Increased runoff and paleolake development, *J. Geophys. Res.*, *110*, E12S15, doi:10.1029/2005JE002460.

Johnson, J. R., F. Hörz, P. G. Lucey, and P. R. Christensen (2002), Thermal infrared spectroscopy of experimentally shocked anorthosite and pyroxenite: Implications for remote sensing of Mars, *J. Geophys. Res.*, *107*(E10), 5073, doi:10.1029/2001JE001517.

Johnson, J. R., M. I. Staid, T. N. Titus, and K. Becker (2006), Shocked plagioclase signatures in Thermal Emission Spectrometer data of Mars, *Icarus*, *180*, 60–74.

Knudson, A. T., and P. R. Christensen (2004), Hematite in Vallis Marineris: Context, composition, distribution, morphology, physical properties and comparison to other Mars hematite deposits, *Eos Trans. AGU*, *85*(47), Fall Meet. Suppl., Abstract P21A-0215.

Koeppen, W. C., and V. E. Hamilton (2005), Discrimination of glass and phyllosilicate minerals in thermal infrared data, *J. Geophys. Res.*, *110*, E08006, doi:10.1029/2005JE002474.

Kraft, M. D., and R. Greeley (2000), Rock coatings and aeolian abrasion on Mars: Application to the Pathfinder landing site, *J. Geophys. Res.*, *105*(E6), 15,107–15,116.

Kraft, M. D., J. R. Michalski, and T. G. Sharp (2003), Effects of pure silica coatings on thermal emission spectra of basaltic rocks: Considerations for Martian surface mineralogy, *Geophys. Res. Lett.*, *30*(24), 2288, doi:10.1029/2003GL018848.

Kraft, M. D., J. R. Michalski, and T. G. Sharp (2005), Palagonite-like alteration products on the Earth and Mars 2: secondary mineralogy of crystalline basalts weathered under semi-arid conditions, *Lunar Planet. Sci.*, *XXXVI*, abstract 1376.

Lawson, C. L., and R. J. Hanson (1974), *Solving Least-Squares Problems*, 340 pp., Prentice-Hall, Upper Saddle River, N. J.

Le Mouélic, S., C. Sotin, J.-P. Combe, L. Ledeit, A. Gendrin, J. Mustard, J.-P. Bibring, Y. Langevin, B. Gondet, and P. Pinet (2006), Composition of the dust on Mars derived from OMEGA hyperspectral images, *Lunar Planet. Sci.*, *XXXVII*, abstract 1409.

Mangold, N., C. Quantin, V. Ansan, C. Delacourt, and P. Allemand (2004), Evidence for precipitation on Mars from dendritic valleys in the Valles Marineris area, *Science*, *305*, 78–81.

Martinez-Alonso, S., M. T. Mellon, B. C. Kindel, and B. M. Jakosky (2006), Mapping compositional diversity on the surface of Mars: The Spectral Variance Index, *J. Geophys. Res.*, *111*, E01004, doi:10.1029/2005JE002492.

McAdam, A. C., M. Y. Zolotov, M. V. Mironenko, L. A. Leshin, and T. G. Sharp (2006), Aqueous chemical weathering of a Mars analog lithology: Kinetic modeling for a ferrar dolerite composition, *Lunar Planet. Sci.*, *XXXVII*, abstract 2363.

McLennan, S. M. (2003), Sedimentary silica on Mars, *Geology*, *31*(4), 315–318.

McSween, H. Y., Jr. (1994), What we have learned about Mars from SNC meteorites, *Meteoritics*, *29*(6), 757–779.

McSween, H. Y., and E. Jarosewich (1983), Petrogenesis of the Elephant Moraine A79001 Meteorite—Multiple magma pulses on the shergottite parent body, *Geochim. Cosmochim. Acta*, *47*(8), 1501–1513.

McSween, H. Y., T. L. Grove, and M. B. Wyatt (2003), Constraints on the composition and petrogenesis of the Martian crust, *J. Geophys. Res.*, *108*(E12), 5135, doi:10.1029/2003JE002175.

McSween, H. Y., et al. (2004), Basaltic rocks analyzed by the Spirit rover in Gusev Crater, *Science*, *305*, 842–845.

McSween, H. Y., et al. (2006), Characterization and petrologic interpretation of olivine-rich basalts at Gusev Crater, Mars, *J. Geophys. Res.*, *111*, E02S10, doi:10.1029/2005JE002477.

Michalski, J. R., M. D. Kraft, T. Diedrich, T. G. Sharp, and P. R. Christensen (2003), Thermal emission spectroscopy of the silica polymorphs and considerations for remote sensing of Mars, *Geophys. Res. Lett.*, *30*(19), 2008, doi:10.1029/2003GL018354.

Michalski, J. R., S. J. Reynolds, T. G. Sharp, and P. R. Christensen (2004), Thermal infrared analysis of weathered granitic rock compositions in the Sacaton Mountains, Arizona: Implications for petrologic classifications from thermal infrared remote-sensing data, *J. Geophys. Res.*, *109*, E03007, doi:10.1029/2003JE002197.

Michalski, J. R., M. D. Kraft, T. G. Sharp, L. B. Williams, and P. R. Christensen (2005a), Mineralogical constraints on the high-silica Martian surface component observed by TES, *Icarus*, *174*(1), 161–177.

Michalski, J. R., M. D. Kraft, T. G. Sharp, and P. R. Christensen (2005b), Palagonite-like alteration products on the Earth and Mars I: Spectroscopy (0.4–2.5 microns) of weathered basalts and silicate alteration products, *Lunar Planet. Sci.*, *XXXVI*, abstract 1188.

Milliken, R. E., J. F. Mustard, and D. L. Goldsby (2003), Viscous flow features on the surface of Mars: Observations from high-resolution Mars Orbiter Camera (MOC) images, *J. Geophys. Res.*, *108*(E6), 5057, doi:10.1029/2002JE002005.

Minitti, M. E., C. M. Weitz, M. D. Lane, and J. L. Bishop (2003), Composition and spectra of several Hawaiian rock coatings, *Lunar Planet. Sci.*, *XXXIV*, abstract 1937.

Minitti, M. E., C. M. Weitz, M. D. Lane, and J. L. Bishop (2005), Rock coatings from Vulcano, a Martian analog environment, *Lunar Planet. Sci.*, *XXXVI*, abstract 1835.

Moersch, J. E., T. L. Hayward, P. D. Nicholson, S. W. Squyres, J. VanCleve, and P. R. Christensen (1997), Identification of a 10-mu m silicate absorption feature in the Acidalia region of Mars, *Icarus*, *126*(1), 183–196.

Morris, R. V., T. G. Graff, S. A. Mertzman, M. D. Lane, and P. R. Christensen (2003), Palagonitic (not andesitic) Mars: Evidence from thermal emission and VNIR spectra of palagonitic alteration rinds on basaltic rock, paper presented at Sixth International Conference on Mars, Calif. Inst. of Technol., Pasadena.

Morse, S. A. (1996), Kiglapait mineralogy: 3. Olivine compositions and Rayleigh fractionation models, *J. Petrol.*, *37*(5), 1037–1061.

Mustard, J. F., and J. M. Sunshine (1995), Seeing through the dust—Martian crustal heterogeneity and links to the SNC meteorites, *Science*, *267*, 1623–1626.

Mustard, J. F., S. Erard, J. P. Bibring, J. W. Head, S. Hurtrez, Y. Langevin, C. M. Pieters, and C. J. Sotin (1993), The surface of Syrtis Major—Composition of the volcanic substrate and mixing with altered dust and soil, *J. Geophys. Res.*, *98*(E2), 3387–3400.

Mustard, J. F., S. Murchie, S. Erard, and J. Sunshine (1997), In situ compositions of Martian volcanics: Implications for the mantle, *J. Geophys. Res.*, *102*(E11), 25,605–25,615.

Mustard, J. F., C. D. Cooper, and M. K. Rifkin (2001), Evidence for recent climate change on Mars from the identification of youthful near-surface ground ice, *Nature*, *412*(6845), 411–414.

Mustard, J. F., F. Poulet, A. Gendrin, J. P. Bibring, Y. Langevin, B. Gondet, N. Mangold, G. Bellucci, and F. Altieri (2005), Olivine and pyroxene diversity in the crust of Mars, *Science*, *307*, 1594–1597.

Piatek, J. L. (1997), Vibrational spectroscopy of clay minerals: implications for remote sensing of terrestrial planetoids, M. S. thesis, Ariz. State Univ., Tempe.

Poulet, F., J. P. Bibring, J. F. Mustard, A. Gendrin, N. Mangold, Y. Langevin, R. E. Arvidson, B. Gondet, and C. Gomez (2005), Phyllosilicates on Mars and implications for early Martian climate, *Nature*, *438*(7068), 623–627.

Ramsey, M. S., and P. R. Christensen (1998), Mineral abundance determination: Quantitative deconvolution of thermal emission spectra, *J. Geophys. Res.*, *103*(B1), 577–596.

Rogers, A. D., P. R. Christensen, and J. L. Bandfield (2005), Compositional heterogeneity of the ancient Martian crust: Surface analysis of Ares Vallis

bedrock with THEMIS and TES data, *J. Geophys. Res.*, *110*, E05010, doi:10.1029/2005JE002399.

Rogers, A. D., J. L. Bandfield, and P. R. Christensen (2007), Global spectral classification of Martian low-albedo regions with MGS-TES data, *J. Geophys. Res.*, doi:10.1029/2006JE002726, in press.

Rogers, D., and P. R. Christensen (2003), Age relationship of basaltic and andesitic surface compositions on Mars: Analysis of high-resolution TES observations of the Northern Hemisphere, *J. Geophys. Res.*, *108*(E4), 5030, doi:10.1029/2002JE001913.

Roush, T. L., D. L. Blaney, and R. B. Singer (1993), The surface composition of Mars as inferred from spectroscopic observations, in *Remote Geochemical Analysis: Elemental and Mineralogical Composition*, edited by C. M. Pieters and P. A. J. Englert, pp. 367–393, Cambridge Univ. Press, New York.

Ruff, S. W. (1998), Quantitative thermal infrared emission spectroscopy applied to granitoid petrology, Ph.D. dissertation, Ariz. State Univ., Tempe.

Ruff, S. W. (2003), Basaltic andesite or weathered basalt: A new assessment, paper presented at Sixth International Conference on Mars, Calif. Inst. of Technol., Pasadena.

Ruff, S. W. (2004), Spectral evidence for zeolite in the dust on Mars, *Icarus*, *168*(1), 131–143.

Ruff, S. W., and the Athena Science Team (2006), The absence and presence of olivine in the Columbia Hills of Gusev Crater, Mars: The latest results from Mini-TES, *Lunar Planet. Sci.*, *XXXVII*, abstract 1989.

Sagan, C. (1973), Sandstorms and eolian erosion on Mars, *J. Geophys. Res.*, *78*(20), 4155–4161.

Scott, D. H., and K. L. Tanaka (1986), Geologic map of the western equatorial region of Mars, 1:15000,000, *U.S. Geol. Surv. Misc. Invest. Map, I-1802-A*.

Seelos, F. P., IV, and R. E. Arvidson (2003), Bounded variable least-squares—Application of a constrained optimization algorithm to the analysis of TES emissivity spectra, *Lunar Planet. Sci.*, *XXXIV*, abstract 1817.

Sharp, R. P., and M. C. Malin (1975), Channels on Mars, Geol, *Soc. Am. Bull.*, *86*(5), 593–609.

Singer, R. B., and T. L. Roush (1985), Analysis of Martian crustal petrology, *Bull. Am. Astron. Soc.*, *17*, 737.

Singer, R. B., T. B. Mccord, R. N. Clark, J. B. Adams, and R. L. Huguenin (1979), Mars surface composition from reflectance spectroscopy: A summary, *J. Geophys. Res.*, *84*(B14), 8415–8426.

Smith, D. E., et al. (2001), Mars Orbiter Laser Altimeter: Experiment summary after the first year of global mapping of Mars, *J. Geophys. Res.*, *106*(E10), 23,689–23,722.

Soderblom, L. A. (1992), The composition and mineralogy of the Martian surface from spectroscopic observations: 0.3 microns to 50 microns, in *Mars*, edited by H. H. Kieffer et al., pp. 557–593, Univ. of Ariz. Press, Tucson.

Solomon, S. C., et al. (2005), New perspectives on ancient Mars, *Science*, *307*, 1214–1220.

Squyres, S. W., et al. (2004), In situ evidence for an ancient aqueous environment at Meridiani Planum, Mars, *Science*, *306*, 1709–1714.

Squyres, S. W., et al. (2006), Rocks of the Columbia Hills, *J. Geophys. Res.*, *111*, E02S11, doi:10.1029/2005JE002562.

Stöffler, D., and F. Langenhorst (1994), Shock metamorphism of quartz in nature and experiment: 1. Basic observation and theory, *Meteoritics*, *29*(2), 155–181.

Stolper, E., and H. Y. McSween (1979), Petrology and origin of the shergottite meteorites, *Geochim. Cosmochim, Acta*, *43*(9), 1475–1498.

Strom, R. G., S. K. Croft, and N. G. Barlow (1992), The Martian impact cratering record, in *Mars*, edited by H. H. Kieffer et al., pp. 383–423, Univ. of Ariz. Press, Tucson.

Tanaka, K. L., and D. H. Scott (1987), Geologic map of the polar regions of Mars, scale 1:15000,000, *U.S. Geol. Surv. Misc. Invest. Ser. Map, I-1802-C*.

Taylor, G. J., L. M. V. Martel, and W. V. Boynton (2006), Mapping Mars geochemically, *Lunar Planet Sci.*, *XXXVII*, abstract 1981.

Taylor, L. A., et al. (2002), Martian meteorite Dhofar 019: A new shergottite, *Meteorit. Planet. Sci.*, *37*(8), 1107–1128.

Tosca, N. J., S. M. McLennan, D. H. Lindsley, and M. A. A. Schoonen (2004), Acid-sulfate weathering of synthetic Martian basalt: The acid fog model revisited, *J. Geophys. Res.*, *109*, E05003, doi:10.1029/2003JE002218.

Treiman, A. H., G. A. Mckay, D. D. Bogard, D. W. Mittlefehldt, M. S. Wang, L. Keller, M. E. Lipschutz, M. M. Lindstrom, and D. Garrison (1994), Comparison of the Lew88516 and Alha77005 Martian Meteorites—Similar but distinct, *Meteoritics*, *29*(5), 581–592.

Wieczorek, M. A., and M. T. Zuber (2004), Thickness of the Martian crust: Improved constraints from geoid-to-topography ratios, *J. Geophys. Res.*, *109*, E01009, doi:10.1029/2003JE002153.

Wright, S. P., J. L. Bandfield, P. R. Christensen, and J. R. Johnson (2004), Removing the shock from the thermal emission spectra of shocked terrestrial and Martian basalts, *Eos Trans. AGU*, *85*(47), Fall Meet. Suppl., Abstract P11A-0954.

Wyatt, M. B., and H. Y. McSween (2002), Spectral evidence for weathered basalt as an alternative to andesite in the northern lowlands of Mars, *Nature*, *417*(6886), 263–266.

Wyatt, M. B., V. E. Hamilton, H. Y. McSween, P. R. Christensen, and L. A. Taylor (2001), Analysis of terrestrial and Martian volcanic compositions using thermal emission spectroscopy: 1. Determination of mineralogy, chemistry, and classification strategies, *J. Geophys. Res.*, *106*(E7), 14,711–14,732.

Wyatt, M. B., H. Y. McSween, K. L. Tanaka, and J. W. Head (2004), Global geologic context for rock types and surface alteration on Mars, *Geology*, *32*(8), 645–648.

Yen, A. S., et al. (2005), An integrated view of the chemistry and mineralogy of Martian soils, *Nature*, *436*(7047), 49–54.

Zipfel, J., P. Scherer, B. Spettel, G. Dreibus, and L. Schultz (2000), Petrology and chemistry of the new shergottite Dar al Gani 476, *Meteorit. Planet. Sci.*, *35*(1), 95–106.

Zuber, M. T. (2001), The crust and mantle of Mars, *Nature*, *412*(6843), 220–227.

Zuber, M. T., et al. (2000), Internal structure and early thermal evolution of Mars from Mars Global Surveyor topography and gravity, *Science*, *287*, 1788–1793.

P. R. Christensen, Department of Geological Sciences, Arizona State University, Campus Box 6305, Tempe, AZ 85287-6305, USA.

A. D. Rogers, Division of Geological and Planetary Sciences, California Institute of Technology, MC 150-21, Pasadena, CA 91125, USA. (drogers@gps.caltech.edu)